AGU PUBLICATIONS

JGR

Journal of Geophysical Research: Oceans

RESEARCH ARTICLE

10.1002/2015JC010712

Key Points:

- We provide simple estimates of the transport by surface wave groups
- The effects of finite depth and directionality are crucial and we show how
- We provide estimates of the depth separating Stokes drift and return flow

Correspondence to:

T. S. van den Bremer,
tonvandenbremer@gmail.com

Citation:

van den Bremer, T. S., and P. H. Taylor (2015), Estimates of Lagrangian transport by surface gravity wave groups: The effects of finite depth and directionality, *J. Geophys. Res. Oceans*, *120*, 2701–2722, doi:10.1002/2015JC010712.

Received 16 JAN 2015
Accepted 13 MAR 2015
Accepted article online 18 MAR 2015
Published online 11 APR 2015

Estimates of Lagrangian transport by surface gravity wave groups: The effects of finite depth and directionality

T. S. van den Bremer[1] and P. H. Taylor[1]

[1]Department of Engineering Science, University of Oxford, Oxford, UK

Abstract Two physical phenomena drive the Lagrangian trajectories of neutrally buoyant particles underneath surface gravity wave groups: the Stokes drift results in a net displacement of particles in the direction of propagation of the group, whereas the Eulerian return flow transports such particles in the opposite direction. Generally, the Stokes drift is the larger of the two near the surface, whereas the effects of the return flow dominate at depth. A transition depth can be defined that separates the two regimes. Using a multiple-scales expansion, we provide leading-order estimates of the forward transport, the backward transport, and the transition depth for realistic sea states. We consider the effects of both finite depth and the directionally spread nature of the waves on our estimates. We show that from the perspective of the return flow, almost all seas are of finite depth. In fact, many seas can be shown to be "shallow" from the perspective of the return flow with little variation of this flow with depth. Furthermore, even small degrees of directional spreading can considerably reduce the magnitude of the return flow and its transport.

1. Introduction

Surface gravity waves have an associated wave-induced mean flow known as the Stokes drift named after George Gabriel *Stokes*, who first derived a theoretical description for this drift in 1847 [*Stokes*, 1847]. The drift manifests itself as the mean horizontal velocity of fluid parcels (Lagrangian particles) that are displaced by a finite horizontal distance over each wave cycle. During one cycle beneath a wave on deep water, at leading order in the steepness of the wave, the particle follows a circular trajectory with the size of the circle decreasing exponentially with depth. At the next order, it is clear these orbits do not close resulting from the displacement of the Lagrangian particle from its initial position:

$$u_{SD}=\overline{\frac{\partial u^{(1)}}{\partial x}\Delta x^{(1)}+\frac{\partial u^{(1)}}{\partial x}\Delta z^{(1)}}, \tag{1}$$

where the over line denotes averaging over the individual waves and the superscripts denote the order in wave steepness. In an Eulerian framework, a surface gravity wave can be shown to have an associated net volume flux resulting from integration of the linear horizontal velocity with depth up to the linear free surface $\eta^{(1)}$, known as the Stokes transport:

$$Q_{ST}=\overline{\int_{-d}^{\eta^{(1)}(x,t)} u^{(1)}(x,z,t)dz}. \tag{2}$$

Real seas consist of a spectrum of different frequency components thus constituting a packet or group structure. Making use of the separation of scales between the fast variation of the individual waves and the slow variation of the group's modulation for a quasi-monochromatic or narrow-banded group, the expressions for the Stokes drift (1) and the Stokes transport (2) still hold. The averaging denoted by the overlines is over the fast scales, the individual waves. The Stokes transport (2) for groups varies with the (square of the) local amplitude of the group and is therefore divergent. It must induce a return flow ($\mathbf{u}_{RF}$) first described by *Longuet-Higgins and Stewart* [1962] that in some sense returns the fluid deposited by the Stokes transport at the group's leading edge to be absorbed again by the Stokes transport at its trailing edge. For sufficiently deep water, a spatial separation of the two effects takes place, as illustrated in Figure 1: Stokes drift dominates near the free surface and the return flow dominates at depth. In physical terms, the dynamic free surface boundary condition, requiring a uniform pressure on the free surface and the satisfaction of

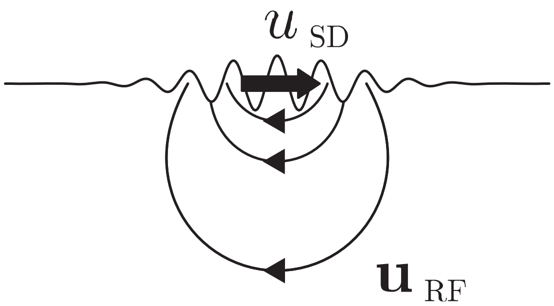

Figure 1. Illustration of the spatial separation between Stokes drift and the return flow for a surface gravity wave group in sufficient depth [see also *McIntyre*, 1981, Figure 2].

Bernoulli's law for energy conservation, prevent a net deposition (extraction) of fluid at the leading (trailing) edge of the group due the horizontal convergence (divergence) of the Stokes transport. Conservation of volume then governs the behavior of the return flow.

Broadly, two oceanographic applications of Stokes drift can be distinguished: its effect on Lagrangian tracers such as pollutants and buoys on the one hand and its part in the physics of the ocean surface mixed layer on the other. Regarding the first, Stokes drift plays an important role in trajectory forecasts for search and rescue operations, oil spill mitigation, and the interpretation of in situ observations obtained from tracking buoys [*Röhrs et al.*, 2013]. These authors use data to estimate the effects on Lagrangian displacement of a submerged tracking buoy (in water depths of 220–700 m) distinguishing the effects of the Stokes drift and the wave-induced Eulerian fluxes as well as the Coriolis-Stokes forcing.

Second, Stokes drift plays an important role in the ocean surface boundary (or "mixed") layer, the approximately 100 m thick layer that controls the exchange of heat, momentum, and gases between the atmosphere and the ocean and is therefore critical in determining the role of the global ocean circulation on climate [see *Belcher et al.*, 2012, for a review]. With lines of constant vorticity moving with Lagrangian fluid particles in an inviscid fluid, the sheared depth profile of the Stokes drift velocity stretches (initially vertically orientated) vorticity into the horizontal plane [*Polton et al.*, 2005]. Two sources of vertical vorticity can be distinguished: the three-dimensional turbulent vorticity that give rise to Langmuir circulation and the planetary vorticity that interacts with the Stokes drift and gives rise to the Stokes-Coriolis force.

With both Langmuir turbulence and the Stokes-Coriolis forcing included in oceanic general circulation models, the magnitude of the Stokes drift and its variation with depth (cf. shear) must also be included. In such models, the individual waves are typically too small to be resolved by even the most powerful computational models and the effect of Stokes drift must be parameterized before inclusion. Such parameterizations have only recently begun to be extended to include the nonmonochromatic or group nature of the waves [*Breivik et al.*, 2014]. These authors propose a deep water approximation of the Stokes drift velocity profile as an alternative to the monochromatic profile and compare to parametric spectra and profiles under wave spectra from the Interim ECMWF Re-Analysis (ERA-Interim) and buoy observations to reveal much better agreement.

An important assumption is often that the sea is deep, in other words, that the product of the wave number k_0 and the water depth d is large, typically taken as $k_0 d \gtrsim 3$. Variation of the (linear) properties can then be assumed to be exponential with depth considerably simplifying the analysis. Whereas the variation of the linear dynamics with depth scales on the inverse of the wave number k_0^{-1}, the return flow varies on the horizontal scale of the wave group σ. For the return flow to be unaffected by the bottom boundary condition, we thus require $d/\sigma = \varepsilon k_0 d$ to be large, a more restrictive assumption. For a quasi-monochromatic group, the parameter $\varepsilon = 1/(k_0\sigma)$ is assumed to be small. A sea that is deep for a $T_0 = 10$ s wave, namely $d \approx 75$ m so that $k_0 d = 3$, may require a much greater depth for the return flow to be unaffected by the bottom boundary condition, namely $d \gtrsim 3$ km (taking $z/\sigma = -20$ as a criterion from Figure 4d with $\varepsilon = 0.16$), as calculations in section 3 of this paper suggest. Furthermore, the magnitudes of the return flow are expected to reduce considerably when the spectrum is directionally spread and the group becomes spatially localized in both horizontal directions. The return flow can then occur around the sides of the group as well as beneath. The motivation for this paper is thus to study the behavior of the return flow and its contribution to Lagrangian transport for realistic sea states: sea states in finite depth and with directional spreading. The effects of the earth's rotation are not considered herein, nor are the effects of surface tension, viscous drag in the boundary layer or turbulent drag in the Ekman layer.

The objective of this paper is to find simple order-of-magnitude estimates of the net transport of Lagrangian particles as a function of depth and of the physically relevant properties of the sea state. An approximate transition depth is proposed, above which Lagrangian particles are transported forward and below which the transport is in the opposite direction. The transition depth is extended to a transition curve for directionally spread seas to indicate the region below the wave group in which particles travel forward. In short, we set out to examine the effect of finite depth and the directional nature of the spectrum in a three-dimensional sea on three quantities: the net horizontal transport by the Stokes drift, the net horizontal transport by the return flow and the transition depth or curve that separates these two regimes.

In order to simplify the problem, we ignore the effect of dispersion, which modifies the shape of the wave group as it translates in the space-time domain. To do so, we pursue a separation of scales expansion, where the fast or short scales represent those associated with the individual waves and the slow or long scales are associated with the group. The small parameter $\varepsilon=1/(k_0\sigma)$ with $k_0=2\pi/\lambda_0$ denoting the wave number of the main frequency component of the spectrum and σ denoting the characteristic length of the group, in which the perturbation expansion is performed, then separates the two scales. Although the expansion is not introduced until section 2, we discuss its physical interpretation here. At leading order in ε, the shape of the surface elevation of the group and, in fact, any linear wave group signal, in an unidirectional problem is given by a relationship of the form $\eta(x,t)=\mathrm{Re}[A(\varepsilon(x-c_{g,0}t))\exp(i(k_0x-\omega_0t))]$ with ω_0, k_0, and $c_{g,0}$ denoting the wave frequency, wave number, and the group velocity of the peak of the spectrum (or the "carrier" wave) of a quasi-monochromatic wave group. For a Gaussian spectrum, we would have $A=a_0\exp(-(x-c_{g,0}t)^2/2\sigma^2)$ or, for the surface elevation in frequency-space $\hat{\eta}(k)=\sqrt{\pi}a_0\sigma\exp(-\sigma^2(k-k_0)^2/4)$. At leading order in the parameter ε, namely in a narrow-banded approximation, the net particle displacement by a single wave group can thus be found by integrating the stationary (in $(x-c_{g,0}t)$) velocity field from $t\to-\infty$ to $t\to\infty$.

Frequency dispersion then acts to change the shape of the group as it translates and comes in at the next order in ε. Leading-order dispersion for a Gaussian group in deep water is described by [*Kinsman*, 1984]:

$$\eta(x,t)=\mathrm{Re}\left[\frac{a_0}{\sqrt{1+\frac{i\gamma_0 t}{\sigma^2}}}e^{-\left(\frac{1}{1+\gamma_0^2t^2/\sigma^4}\frac{(x-c_{g,0}t)^2}{2\sigma^2}\right)}e^{i\left(\frac{\gamma_0t/\sigma^2}{1+\gamma_0^2t^2/\sigma^4}\frac{(x-c_{g,0}t)^2}{2\sigma^2}\right)}\right], \quad (3)$$

where $\gamma_0=d^2\omega/dk^2|_{k=k_0}=-\sqrt{g/k_0^3}/4$ with $\omega(k)$ obtained from the linear dispersion relationship. As time progresses, the group thus becomes wider and less high due to dispersion in addition to a change in phase. From (3), a characteristic time scale for translation $T_\mathrm{T}\equiv\sigma/c_{g,0}$ and a characteristic time scale for dispersion $T_\mathrm{D}\equiv\sigma^2/|\gamma_0|$ can be obtained. The ratio of the two time scales is then given by $T_\mathrm{D}/T_\mathrm{T}=2/\varepsilon$, a number that is typically large for ε small. For $\varepsilon=0.16$, a representative value obtained from fitting an idealized Gaussian spectrum to the enhanced peak of a Jonswap spectrum [*Gibbs and Taylor*, 2005], we have $T_\mathrm{D}/T_\mathrm{T}=2/\varepsilon\approx12.5$. In practice, the effect on particle displacement is even smaller as the reduction in height and the widening of the group in (3) act in opposite directions. The effect of dispersion is even smaller for finite water depth and the leading-order wave group representation becomes an effective replacement of multichromatic wave theories such as those by *Longuet-Higgins and Stewart* [1962], *Sharma and Dean* [1981], or *Dalzell* [1999], which include all orders in ε. Most importantly, these leading-order wave group representations are amenable to simple closed-form solutions for the net displacements pursued herein.

This paper is laid out as follows. Section 2 introduces the governing equations and boundary conditions and formally introduces the approximation method by examining the simplest case: a two-dimensional sea of infinite depth. Section 3 considers the effects of finite depth for two-dimensional seas, followed by a discussion of three-dimensional effects in section 4, with realistic directional distributions being considered in section 4.3. Finally, conclusions are drawn in section 5.

2. Governing Equations and Separation of Scales Model

2.1. Governing Equations

Assuming irrotational and incompressible flow in a fluid of constant density, the governing equation $\nabla^2\phi=0$ can be expressed in terms of the velocity potential ϕ defined here in a three-dimensional coordinate system (x, y, z) with velocity components $u=\partial\phi/\partial x$, $v=\partial\phi/\partial y$, and $w=\partial\phi/\partial z$. In vector notation, we have $\mathbf{x}=(x,y,z)$ and $\mathbf{u}=(u,v,w)$. Gravity $\mathbf{g}$ acts in the negative z direction and the still water level corresponds to

$z=0$. The governing equation is solved subject to the linear no-flow bottom boundary condition $w(z=-d)=0$ and the kinematic and dynamic boundary conditions at the free surface $z=\eta(x,y,t)$:

$$\frac{D}{Dt}(\eta(x,y,t)-z)=0, \tag{4a}$$

$$g\eta+\frac{\partial\phi}{\partial t}+\frac{1}{2}(\nabla\phi)^2=0 \text{ at } z=\eta, \tag{4b}$$

where $D/Dt=\partial_t+\mathbf{u}\cdot\nabla$ denotes a total derivative and $(\nabla\phi)^2\equiv(\nabla\phi)\cdot(\nabla\phi)=u^2+v^2+w^2$ the inner product.

2.2. A Leading-Order Two-Dimensional Separation of Scales Model for Deep Water

Two small parameters can be defined: the steepness $\alpha=k_0|a_0|$, the product of a characteristic wave number k_0, and the magnitude of the amplitude $|a_0|=||A(X)||$ of the surface elevation envelope $A(X)$, and a bandwidth parameter $\varepsilon=1/(k_0\sigma)$, a measure of the bandwidth of the spectrum with $\varepsilon\to 0$ corresponding to a periodic wave and σ an estimate of the characteristic spatial scale of the group. In the deep water limit ($d\to-\infty$) and a two-dimensional sea, the dimensional linear signal ($O(\alpha^1\varepsilon^0)$) is given by:

$$\eta^{(1)}=A(X)e^{i(k_0x-\omega_0t)}, \tag{5a}$$

$$\phi^{(1)}=B(X,Z)e^{k_0z}e^{i(k_0x-\omega_0t)}, \tag{5b}$$

where the real part is understood. The envelopes $A(X)$ (L) and $B(X, Z)$ (L^2T^{-1}) are functions of the slow scales:

$$X=\varepsilon(x-c_{g,0}t), \tag{6a}$$

$$Z=\varepsilon z, \tag{6b}$$

where the linear dispersion equation $\omega_0^2=gk_0$, $c_{g,0}=d\omega_0/dk_0=\sqrt{g/k_0}/2$, and $A=i(k_0/\omega_0)B|_{z=0}$ ensure the linear (in α) parts of the boundary conditions ((4a) and (4b)) are satisfied (at zeroth and first order in ε). The slow depth scale Z is required to ensure that the Laplace equation is satisfied at first (and subsequent) order(s) in ε.

The Stokes drift, defined as the net horizontal velocity of a Lagrangian particle due to the linear wave motion (1), and the Stokes transport, defined as the net depth-integrated horizontal Eulerian volume flux associated with linear wave motion (2), are given by:

$$u_{\mathrm{SD}}=\omega_0k_0e^{2k_0z}|A(X)|^2, \tag{7a}$$

$$Q_{\mathrm{ST}}=\frac{1}{2}\omega_0|A(X)|^2. \tag{7b}$$

At leading order in ε, the return flow is forced by the divergence of the Stokes transport:

$$\frac{\partial\phi_{\mathrm{RF}}}{\partial z}=\varepsilon\frac{\partial Q_{\mathrm{ST}}}{\partial X} \quad \text{at } z=0, \tag{8}$$

which can be obtained from combination of (4a) and (4b), substitution of the linear solutions (5a) and (5b) and averaging over the fast scales. The physical interpretation of (8) is that the divergence of the Stokes transport on the right-hand side has to be balanced by a down-flowing return flow on the leading edge of the group and a up-flowing return flow on its trailing edge. The return flow is governed by Laplace $\nabla^2\phi_{\mathrm{RF}}=0$, subject to the bottom boundary condition $w_{\mathrm{RF}}\to 0$ as $z\to-\infty$ and the "forcing" equation (8), to give for the horizontal velocity:

$$u_{\mathrm{RF}}=-\frac{\omega_0|a_0|^2}{2\pi\sigma}\int_0^\infty \hat{k}f(\hat{k})e^{\hat{k}\hat{z}}\cos(\hat{k}\hat{x})d\hat{k}, \tag{9}$$

where the hats denote nondimensional variables, $\hat{k}=k\sigma$, $\hat{z}=z/\sigma$, $\hat{x}=(x-c_{g,0}t)/\sigma$ defined as the horizontal coordinate centered around the middle of the wave group, and $f(\hat{k})$ is the normalized Fourier transform of the squared amplitude envelope:

$$f(\hat{k})=\frac{\int_{-\infty}^{\infty}|A(x)|^2 e^{-ikx}dx}{\sigma|a_0|^2}. \tag{10}$$

For a Gaussian group, $A=|a_0|\exp(-\hat{x}^2/2),\ f(\hat{k})=\sqrt{\pi}\exp(-\hat{k}^2/4)$. In the far-field ($|x-c_{g,0}t|\gg\sigma,\ |z|\gg\sigma$ or both), we can obtain a dipole approximation to the horizontal velocity field. For a Gaussian group, we have from (9) (see Appendix B1):

$$u_{\mathrm{RF}}=\frac{1}{2\sqrt{\pi}}\frac{\omega_0|a_0|^2}{\sigma}\frac{\hat{x}^2-\hat{z}^2}{(\hat{x}^2+\hat{z}^2)^2}. \tag{11}$$

At the center of the group $\hat{x}=0$, the horizontal velocity thus decays as $(z/\sigma)^{-2}$ with depth.

2.2.1. Lagrangian Transport

The total Lagrangian velocity of a particle $\mathbf{u}_{\mathrm{L}}$ is determined by the sum of its Stokes drift $\mathbf{u}_{\mathrm{SD}}$, a Lagrangian phenomenon, and the Eulerian return flow field $\mathbf{u}_{\mathrm{RF}}$:

$$\underbrace{\mathbf{u}_{\mathrm{L}}}_{\text{Lagrangian}}=\underbrace{\mathbf{u}_{\mathrm{SD}}}_{\text{Stokesdrift}}+\underbrace{\mathbf{u}_{\mathrm{RF}}}_{\text{Eulerian}}. \tag{12}$$

The net horizontal displacement by the Stokes drift (7) for a particle as a function of its initial vertical position z_0 and for a Gaussian group is given by:

$$\Delta x_{\mathrm{SD}}(z_0)=2\sqrt{\pi}\sigma\alpha^2 e^{2k_0 z_0}. \tag{13}$$

The net horizontal transport by the return flow can be found by integrating the horizontal return flow velocity (9) with respect to time. For a wave group with the slow effects of dispersion ignored we obtain from (9):

$$\Delta x_{\mathrm{RF}}(z_0)=-\frac{\alpha^2}{\pi k_0}\int_{-\infty}^{\infty}\int_0^{\infty}\hat{k}f(\hat{k})e^{\hat{k}\hat{z}_0}\cos(\hat{k}\hat{t})d\hat{k}d\hat{t}, \tag{14}$$

where the double integral on the right-hand side is nondimensional ($\hat{t}=c_{g,0}t/\sigma$) and only a function of the scaled initial particle depth $\hat{z}_0=z_0/\sigma$. Explicitly, we have from numerical evaluation of the double integral for a particle located at $z_0=0$ and a Gaussian group $\Delta x_{\mathrm{RF}}(z_0=0)\approx-0.1134\alpha^2/k_0$. Comparing magnitudes, we thus have at the surface:

$$\Delta x_{\mathrm{L}}(z_0=0)\approx\sigma\alpha^2(2\sqrt{\pi}-0.1134\varepsilon). \tag{15}$$

For $\varepsilon=0.16$, a representative value obtained from fitting an idealized Gaussian spectrum to the peak of a Jonswap spectrum [*Gibbs and Taylor*, 2005], the contribution due to Stokes drift is a factor $\sim$200 larger than the contribution due to the return flow, provided the sea is two-dimensional and the depth is large relative to both the length of the individual waves λ_0 and the length of the group σ.

2.2.2. The Transition Depth

The transition depth, below which Lagrangian particles are transported backward by the return flow and above which such particles are transported forward by Stokes drift, is defined by:

$$\Delta x_{\mathrm{L}}(z_0=z_{\mathrm{T}})=\Delta x_{\mathrm{SD}}(z_{\mathrm{T}})+\Delta x_{\mathrm{RF}}(z_{\mathrm{T}})=0. \tag{16}$$

Ignoring the generally small effects of dispersion and making use of the fact that Stokes drift decays much faster with depth than the return flow for deep water, an approximate expression for the transition depth z_{T}^* can be obtained. This is achieved by finding the depth at which the net horizontal Stokes drift displacement (13) has decreased to the surface value ($z_0=0$) of the return flow displacement, which can be assumed not to decay over that same depth:

$$\Delta x_{\mathrm{RF}}(z_0=0)+\Delta x_{\mathrm{SD}}(z_0=z_{\mathrm{T,DRF}}^*)=0, \tag{17}$$

which has the solution:

$$z_{\mathrm{T,DRF}}^*\approx\frac{1}{2k_0}(-3.442+\log(\varepsilon)). \tag{18}$$

Derivation of (18) relies on only taking into account the leading-order (in ε) contribution of Stokes drift and the return flow to net horizontal particle transport. Provided the water is deep $(d/\sigma \gg 1)$, the Stokes drift then varies much more rapidly with depth than the return flow and the assumption made to derive (18) is justified. Comparison of (18) with finite depth solutions is made in section 3 to ascertain its range of validity.

3. The Effect of Finite Depth

It is evident from (9) that for the return flow not to feel the effect of finite depth, not only $k_0 d$ needs to be large, but so does $d/\sigma = \varepsilon k_0 d$, which is one order in ε smaller than the former. Without taking the $d \to -\infty$ limit, the linear solution ($O(\alpha^1\varepsilon^0)$) in (5) becomes:

$$\eta^{(1)} = A(X)e^{i(k_0 x - \omega_0 t)}, \tag{19a}$$

$$\phi^{(1)} = B(X,Z)\frac{\cosh\left(k_0(z+d)\right)}{\cosh\left(k_0 d\right)}e^{i(k_0 x - \omega_0 t)}, \tag{19b}$$

where the slow scales are defined as in (6). From the linear ($O(\alpha^1\varepsilon^0)$) free surface boundary conditions (4a) and (4b) we have $B|_{z=0} = -igA/\omega_0$ and $\omega_0^2 = gk_0\tanh\left(k_0 d\right)$, the linear dispersion relationship. At next order in ε, the linear (in α) signals are defined such that the envelope travels at the group velocity $c_{g,0} = d\omega_0/dk_0$.

From the linear signal (19), leading-order expressions for the Stokes drift and the Stokes transport can be obtained:

$$u_{\mathrm{SD}} = \frac{\omega_0 k_0}{2}\frac{\cosh\left(2k_0(d+z)\right)}{\sinh^2(k_0 d)}|A(X)|^2, \tag{20a}$$

$$Q_{\mathrm{ST}} = \frac{\omega_0}{2\tanh\left(k_0 d\right)}|A(X)|^2. \tag{20b}$$

It is evident then from (20) and from Figure 2a, which shows the variation of the Stokes drift with depth for a number of different depths, that both the magnitude of the Stokes drift and that of the Stokes transport are larger for shallower depth, the latter equal in magnitude to the depth integral of the former.

At second order in steepness, the free surface boundary conditions (4a) and (4b) can be combined to give a "forcing" equation for the Eulerian flow field at second order:

$$\left(\frac{\partial}{\partial z} + \frac{1}{g}\frac{\partial^2}{\partial t^2}\right)\phi^{(2)}_{\mathrm{RF}} = \overline{\underbrace{\nabla_H \cdot \left(\mathbf{u}^{(1)}\eta^{(1)}\right)}_{\nabla_H \cdot \mathbf{Q}_{\mathrm{ST}}} \underbrace{- \frac{1}{g}\frac{\partial}{\partial t}\left(\frac{\partial^2\phi^{(1)}}{\partial t \partial z}\eta^{(1)} + \frac{(\nabla\phi^{(1)})^2}{2}\right)}_{\partial\eta^{(2)}/\partial t}} \text{ at } z=0, \tag{21}$$

where we have used $\partial_z w = -\partial_x u - \partial_y v$ from conservation of volume and $\nabla_H = (\partial_x, \partial_y, 0)$. Equation (21) is referred to as the Eulerian flow forcing equation and constitutes the boundary condition subject to which the Laplace equation has to be solved to obtain the Eulerian flow at second order. Implicitly, we only include terms that contribute to the mean flow here. Hence, the terms on the right-hand side are averaged over the fast scales. The forcing consists of two terms: the divergence of the Stokes transport ($\nabla_H \cdot \mathbf{Q}_{\mathrm{ST}}$) and the variation of the slowly varying set-down of the free surface associated with the group ($\partial\eta^{(2)}/\partial t$). We will refer to the mean flow driven by both these effects as the return flow.

It can be readily verified from the polarization relationships of the linear wave solutions ($O(\alpha^1\varepsilon^0)$), showing the relative phases of the different linear components that only the first term of the mean flow forcing equation ($\nabla_H \cdot \mathbf{Q}_{\mathrm{ST}}$) is nonzero at leading-order ($O(\alpha^2\varepsilon^1)$) for deep water. In words, the mean set-down associated with the group is too small to nonnegligibly affect the underlying mean flow field when the fluid is deep and we assume a slowly varying wave packet. The free surface then "appears rigid to the local mean flow," as observed by *McIntyre* [1981, p. 339] based on taking a limit of the solutions by *Longuet-Higgins and Stewart* [1962]. When the fluid is of finite depth, both terms contribute and we have for the set-down ($O(\alpha^2\varepsilon^0)$) and the return flow potential at leading order ($O(\alpha^2\varepsilon^1)$):

$$\eta^{(2)} = -\frac{1}{2\sinh\left(2k_0 d\right)}k_0 A^2, \tag{22}$$

Journal of Geophysical Research: Oceans 10.1002/2015JC010712

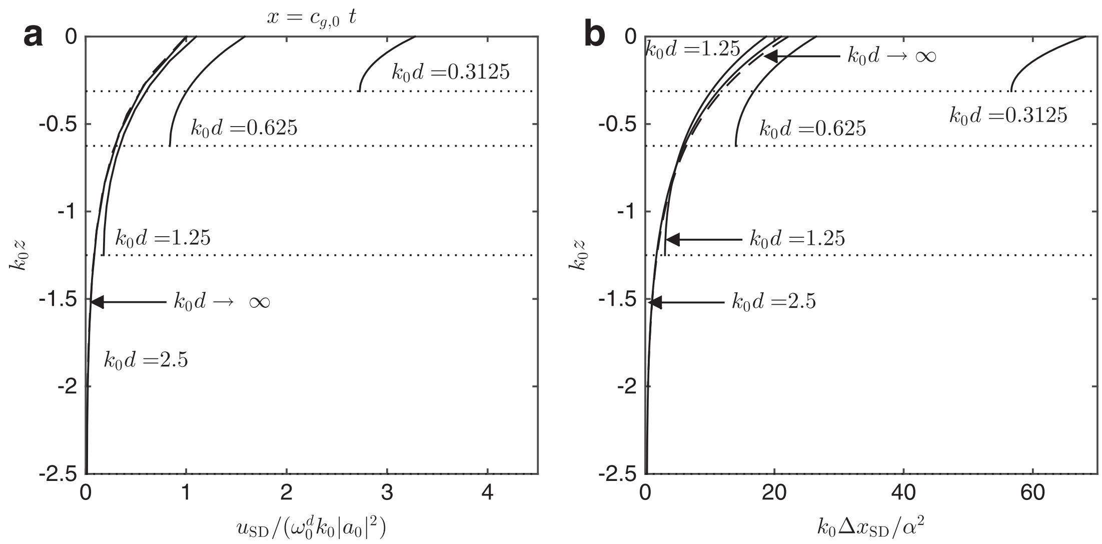

Figure 2. (a) Depth decay of the Stokes drift velocity (20a) and (b) its associated net horizontal transport (27) for different values of the nondimensional depth $k_0 d = \{\infty, 2.5, 1.25, 0.625, 0.3125\}$ ($d/\sigma = \{\infty, 0.4, 0.2, 0.1, 0.05\}$ for $\varepsilon = 0.16$) for a Gaussian group. The asymptotic limits for infinite depth $k_0 d \to \infty$ ((7a) and (27)) are denoted by a dashed lines. The values are correct for two-dimensional seas ((7a) and (20a) in Figure 2a and (13) and (27) in Figure 2b) as well as for three-dimensional seas ((34a) and (46) in Figure 2a and (40) and (50) in Figure 2b) at the center of the group ($y = 0$). To enable comparison in Figure 2a, the wave number $\omega_0^d = \sqrt{g k_0}$ used in the scaling of the horizontal axis is the deep water value, so not a function of depth.

$$\frac{\partial \phi_{\mathrm{RF}}}{\partial z}\bigg|_{z=0} = (1 + \delta_{\mathrm{FD}}(k_0 d)) \frac{\partial Q_{\mathrm{ST}}}{\partial x}, \tag{23}$$

where Q_{ST} is given by (20b) and $\delta_{\mathrm{FD}}(k_0 d) = c_{g,0}\omega_0 / (g \sinh(2k_0 d))$. Explicitly, the term arising from the mean set-down $\delta_{\mathrm{FD}}(k_0 d)$ can be written as:

$$\delta_{\mathrm{FD}}(k_0 d) = \frac{k_0 d \,\mathrm{sech}^2(k_0 d) + \tanh(k_0 d)}{2\sinh(2k_0 d)}. \tag{24}$$

In the deep water limit $k_0 d \to \infty$, $\delta_{\mathrm{FD}}(k_0 d) \to 0$, and we recover the deep water return flow forcing equation (8). In the limit $k_0 d \to 0$, $\delta_{\mathrm{FD}}(k_0 d) \to 1/2$. The corresponding set-down for deep water is $\eta^{(2)} = -\varepsilon k_0 A^2/4$, one order higher in ε than (22).

Solving the boundary value problem subject to the bottom boundary condition and the new forcing equation (23), we obtain for the return flow:

$$u_{\mathrm{RF}} = \frac{-\omega_0 |a_0|^2 (1 + \delta_{\mathrm{FD}}(k_0 d))}{2\pi\sigma \tanh(k_0 d)} \int_0^\infty \frac{\hat{k} f(\hat{k}) \cosh(\hat{k}(\hat{z} + \hat{d}))}{\sinh(\hat{k}\hat{d})} \cos(\hat{k}\hat{x}) d\hat{k}, \tag{25}$$

where $\hat{d} = d/\sigma$ is an additional nondimensional parameter and $f(\hat{k})$ is defined as in (10). By taking the limit $d/\sigma \gg 1$ (and hence $k_0 d \gg 1$), we recover the deep water limit (9). With ε small, it is however possible for the water to be shallow with respect to the return flow which varies on the scale σ but of intermediate depth or even deep with respect to the individual waves that scale on $\lambda_0 = 2\pi/k_0$ (the shallow-water limit $k_0 d \to 0$ is considered in Appendix A for completeness). In this limit ($\hat{d} = d/\sigma \to 0$), (25) reduces to a uniform flow:

$$u_{\mathrm{RF}} = -\frac{\omega_0 |A(X)|^2 (1 + \delta_{\mathrm{FD}}(k_0 d))}{2\tanh(k_0 d) d}, \tag{26}$$

for a general spectrum. Figure 3 compares the horizontal velocity (25) for different depths with the shallow return flow limit (26) at two different locations: at the center of the group $x = c_{g,0}t$ and at the trailing and leading edge $x = c_{g,0}t \pm \sqrt{2}\sigma$.

3.1. Lagrangian Transport

For the net horizontal displacement due to Stokes drift by a Gaussian group, we obtain from (20a) as a function of the initial vertical position of the particle z_0:

AGU Journal of Geophysical Research: Oceans 10.1002/2015JC010712

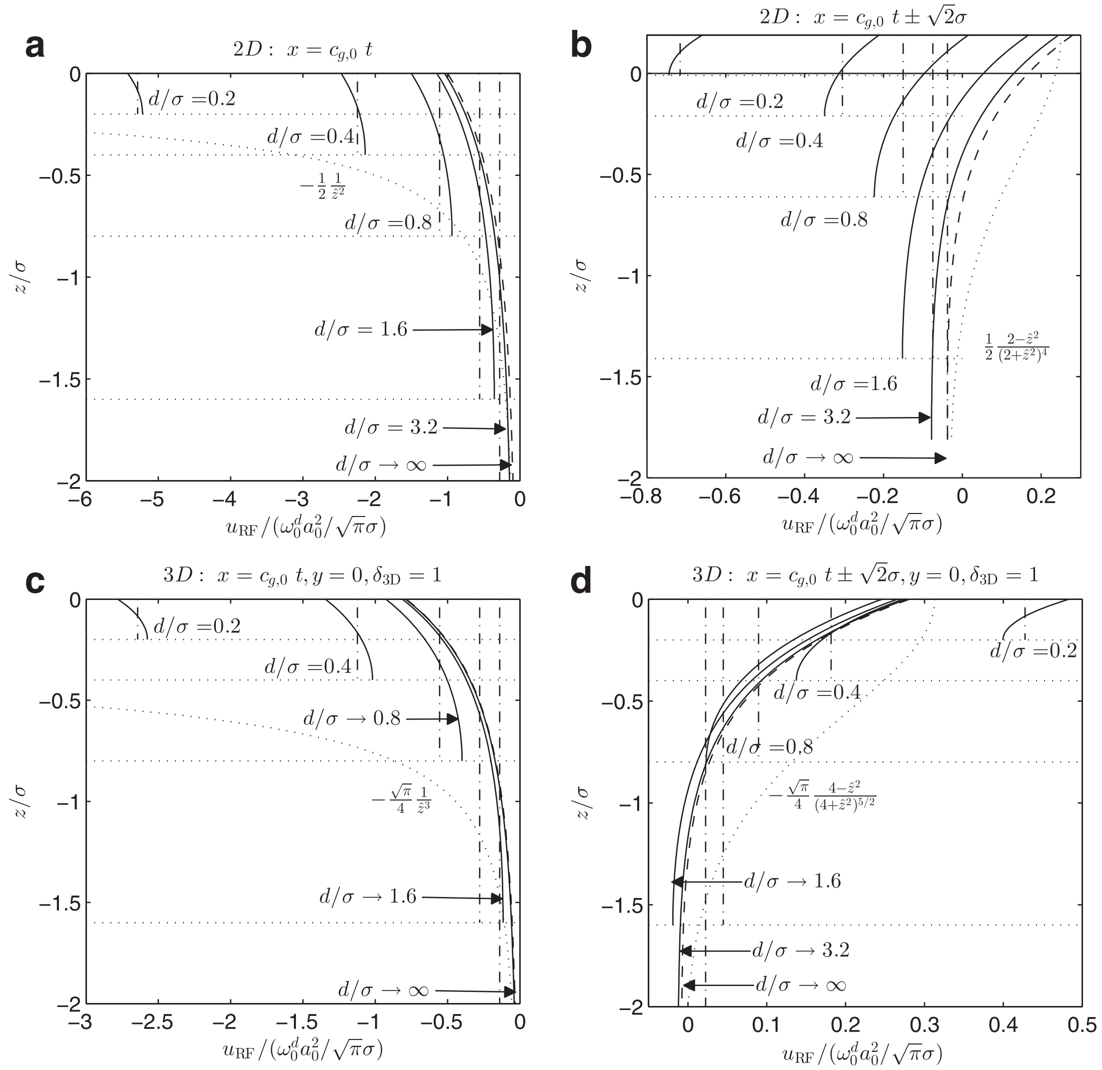

Figure 3. Depth decay of the return flow for (a and b) two-dimensional groups and (c and d) three-dimensional groups with equal group widths in both directions ($\sigma=\sigma_x=\sigma_y$) (a and c) at the center of the group and (b and d) at its edges. The different lines correspond to different depths $d/\sigma=\{\infty, 3.2, 1.6, 0.8, 0.4, 0.2\}$ ($k_0d=\{\infty, 20, 10, 5, 2.5, 1.25\}$ for $\varepsilon=0.16$). The deep water limit ($d/\sigma\to\infty$) is denoted by a dashed line and the shallow return flow limits ((26) and (49)) are denoted by dash-dotted lines.

$$\Delta x_{\mathrm{SD}}(z_0)=2\sqrt{\pi}\alpha^2\sigma\delta_{\mathrm{SD}}(k_0d)\cosh\left(2k_0(d+z_0)\right), \tag{27}$$

where $\delta_{\mathrm{SD}}(k_0d)=\coth(k_0d)/(2k_0d+\sinh(2k_0d))$, so that we have $\delta_{\mathrm{SD}}(k_0d)\cosh(2k_0(d+z))\to\exp(2k_0z)$ as $k_0d\to\infty$ and we recover the deep water limit (13). Figure 2b examines the depth decay of the net displacement by Stokes drift for different values of k_0d. The overall form is of course very similar to the Stokes drift velocity profiles in Figure 2a.

From (25), we have for the net horizontal displacement by the return flow as a function of the initial vertical position of the particle z_0:

$$\Delta x_{\mathrm{RF}}=\frac{-\alpha^2\delta_{\mathrm{RF}}(k_0d)}{\pi k_0}\int_{-\infty}^{\infty}\int_0^{\infty}\frac{\hat{k}f(\hat{k})\cosh(\hat{k}(\hat{z}_0+\hat{d}))}{\sinh(\hat{k}\hat{d})}\cos(\hat{k}\hat{t})d\hat{k}d\hat{t}, \tag{28}$$

where $\delta_{\mathrm{RF}}(k_0d)=\delta_{\mathrm{SD}}(k_0d)(1+\delta_{\mathrm{FD}}(k_0d))\sinh(2k_0d)$ so that $\delta_{\mathrm{RF}}(k_0d)\to1$ as $k_0d\to\infty$ and we recover (14). Explicitly, we have for $\delta_{\mathrm{RF}}(k_0d)$:

$$\delta_{\mathrm{RF}}(k_0d)\quad=\delta_{\mathrm{SD}}(k_0d)(1+\delta_{\mathrm{FD}}(k_0d))\sinh(2k_0d)=\frac{2k_0d+3\sinh(2k_0d)+\sinh(4k_0d)}{2\sinh^2(k_0d)(2k_0d+\sinh(2k_0d))}. \tag{29}$$

If the depth is sufficiently small ($d/\sigma\to0$), (28) reduces to:

$$\Delta x_{\mathrm{RF}} = -2\sqrt{\pi}\alpha^2\sigma\frac{\delta_{\mathrm{RF}}(k_0d)}{2k_0d}. \tag{30}$$

We note that in this shallow-water regime, the net displacement is a (linear) function of σ, whereas for deep water there is no dependence on σ apart from through the dependence on depth $\hat{z}=z/\sigma$ (cf. (14)). In other words, unlike in the deep water case, the net displacement by Stokes drift (27) and by the return flow (30) scale equivalently, namely with σ. The net displacement is evidently no longer a function of the initial vertical particle position. Figure 4 shows the variation of the net horizontal displacement (28) by the return flow as a function as a function of depth. Comparison with the shallow return flow limit (30) confirms that the return flow can be approximated as a shallow uniform flow for all except for extremely large depths.

3.2. The Transition Depth

Although it is not possible to develop an explicit expression for the transition depth for general depth k_0d, the expression for the net transport in the limit in which the water is shallow with respect to the return flow (30) but not with respect to the individual waves (28) gives:

$$\Delta x_{\mathrm{L}} = 2\sqrt{\pi}\alpha^2\sigma\delta_{\mathrm{SD}}(k_0d)\left(\cosh(2k_0(z_0+d)) - \frac{\sinh(2k_0d)(1+\delta_{\mathrm{FD}}(k_0d))}{2k_0d}\right). \tag{31}$$

We can obtain a corresponding estimate of the transition depth by setting $\Delta x_{\mathrm{L}}=0$:

$$z^*_{\mathrm{T,SRF}} = \frac{1}{2k_0}\cosh^{-1}\left(\frac{\sinh(2k_0d)}{2k_0d}(1+\delta_{\mathrm{FD}}(k_0d))\right) - d. \tag{32}$$

Figure 5 compares this approximate transition depth (32) to the implicit solution of $\Delta x_{\mathrm{L}}(z_{\mathrm{T}})=0$ showing the large domain validity of the shallow return flow approximation of the transition depth (32).

Furthermore, it is evident from (23) that for sufficiently small depth, when both the Stokes drift and the return flow start to behave like a uniform flow with depth (see Appendix A), the return flow becomes larger than the Stokes drift. In this limit, the effect of the set-down remains. Setting $z^*_{\mathrm{T,SRF}}=0$, (32) can be solved implicitly to give $k_0d \approx 0.53$ independently of the spectrum as an approximate criterion for $\Delta x_{\mathrm{SD}} = -\Delta x_{\mathrm{RF}}$ at $z_0=0$, the water depth d below which the return flow dominates the Stokes drift at all depth z. The transition depth in Figure 5 is thus only shown for $k_0d > 0.53$.

4. The Effect of Directionality

Realistic sea states are directionally spread and comparison with field measurements by *Donelan et al.* [1985] and *Ewans* [1998] to a wrapped normal distribution gives a root-mean-square spreading parameter of 15°–30° [*Gibbs and Taylor*, 2005]. Assuming the spreading angle is small, we assume the root-mean-square spreading parameter (in radians) corresponds directly to the ratio of the two horizontal scales of the group σ_x and σ_y. We then have $\delta_{3\mathrm{D}} \equiv \sigma_x/\sigma_y = 1.6-3.3$. In order to make analytical progress, we assume the effect of directionality is sufficiently small for it to only affect the slow dynamics. Defining two small parameters $\varepsilon_x = 1/(k_0\sigma_x)$ and $\varepsilon_y = 1/(k_0\sigma_y)$, where k_0 remains the wave number of the fast waves in the x direction, we assume $O(\varepsilon_x)=O(\varepsilon_x)$, but not necessarily $\varepsilon_x=\varepsilon_y$. For root-mean-square spreading parameters toward the lower end of the range 15°–30° this assumption is evidently supported by the data. We have $\varepsilon_y = 0.26-0.52$, setting $\varepsilon_x = 0.16$. In words, the group is typically somewhat longer than it is wide, but, more importantly, the length scales are of the same order of magnitude. To study the effect of introducing a third dimension in the simplest possible way, sections 4.1 and 4.2 initially proceed under the assumption that $\sigma_y=\sigma_x$ (and $\delta_{3\mathrm{D}}=1$). Section 4.3 then relaxes this assumption and examines different degrees of spreading within the reported range. Corresponding solutions for $\delta_{3\mathrm{D}} \neq 1$ are given in Appendix C.

4.1. Infinite Depth ($\sigma_y=\sigma_x$)

In the deep water limit ($d\to\infty$) and a three-dimensional sea (x, y, z), the linear signal ($O(\alpha^1\varepsilon^0)$) is given by:

$$\eta^{(1)} = A(X,Y)e^{i(k_0x-\omega_0t)}, \tag{33a}$$

$$\phi^{(1)} = B(X,Y,Z)e^{k_0z}e^{i(k_0x-\omega_0t)}, \tag{33b}$$

where we have defined an additional slow scale $Y=\varepsilon_y y$ with $\varepsilon_y=1/(k_0\sigma_y)$ and we have assumed the fast carrier wave travels in the x direction without loss of generality. As for the previous section, in which we

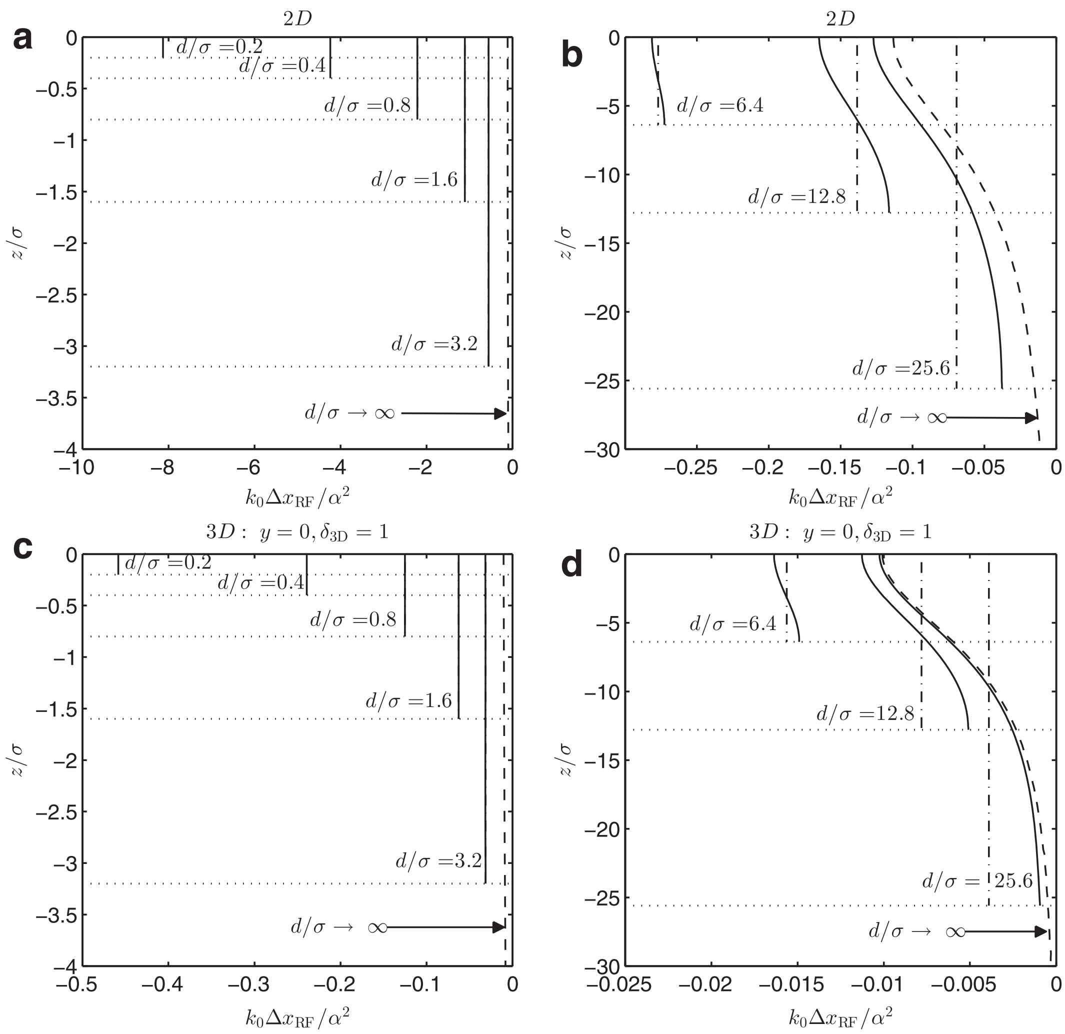

Figure 4. Depth decay of the net horizontal transport by the return flow for different depths for (a and b) two-dimensional groups and (c and d) three-dimensional groups with equal group widths in both directions ($\sigma = \sigma_x = \sigma_y$). The plots on the left show intermediate values of depth $d/\sigma = \{3.2, 1.6, 0.8, 0.4, 0.2\}$ ($k_0 d = \{20, 10, 5, 2.5, 1.25\}$ for $\varepsilon = 0.16$) and the plots on the right show very large depths $d/\sigma = \{\infty, 25.6, 12.8, 6.4\}$ ($k_0 d = \{\infty, 160, 80, 40\}$ for $\varepsilon = 0.16$). Also shown (dash-dotted lines) is the shallow return flow limit (30). The difference is only visible for really large depths (right plots).

have modeled a wave group by considering the leading-order term in a separation of scales expansion between the scales of the group and the scales of the individual waves, we only consider the leading-order effect of directionality here. In (32), we thus have the peak of the directional and frequency spectrum with wave number k_0 traveling in the x direction and consider perturbations away from this in both the directional and the frequency component of the spectrum. For unidirectional seas, we have $\delta_{3D} = 0$ ($\sigma_y \to \infty$) and we return to the two-dimensional solutions presented above. To simplify the analysis, we start by considering the case of a group that is as wide as it is long: $\sigma \equiv \sigma_x = \sigma_y$, $\delta_{3D} = 1$, and thus $\varepsilon = \varepsilon_x = \varepsilon_y$. Section 4.3 considers more realistic directional distributions.

We have for the Stokes drift and the Stokes transport per unit width at leading order:

$$u_{SD} = \omega_0 k_0 e^{2k_0 z} |A(X, Y)|^2, \quad Q_{ST} = \frac{1}{2}\omega_0 |A(X, Y)|^2, \tag{34}$$

where the only difference with the two-dimensional result (7) is the additional dependence on the slow scale Y. We note that at leading order there is only a Stokes drift and transport in the x direction. Although the Stokes drift and Stokes transport are unaffected at leading order in ε ($v^{(1)} = \partial\phi^{(1)}/\partial y = 0$ at $O(\varepsilon^0)$), the return flow is affected at leading order by the introduction of the third dimension. The "forcing" equation (8) remains unchanged, but the governing equation has an additional dimension and we thus have for the return flow:

$$u_{\mathrm{RF}}=-\frac{\omega_0|a_0|^2}{8\pi^2\sigma}\int_{-\infty}^{\infty}\int_{-\infty}^{\infty}\frac{\hat{k}^2 f(\hat{k},\hat{l})}{\sqrt{\hat{k}^2+\hat{l}^2}}e^{\sqrt{\hat{k}^2+\hat{l}^2}\hat{z}+i(\hat{k}\hat{x}+\hat{l}\hat{y})}d\hat{k}d\hat{l}, \tag{35}$$

$$v_{\mathrm{RF}}=-\frac{\omega_0|a_0|^2}{8\pi^2\sigma}\int_{-\infty}^{\infty}\int_{-\infty}^{\infty}\frac{\hat{k}\hat{l} f(\hat{k},\hat{l})}{\sqrt{\hat{k}^2+\hat{l}^2}}e^{\sqrt{\hat{k}^2+\hat{l}^2}\hat{z}+i(\hat{k}\hat{x}+\hat{l}\hat{y})}d\hat{k}d\hat{l}, \tag{36}$$

$$w_{\mathrm{RF}}=\frac{\omega_0|a_0|^2}{8\pi^2\sigma}\int_{-\infty}^{\infty}\int_{-\infty}^{\infty}i\hat{k}f(\hat{k},\hat{l})e^{\sqrt{\hat{k}^2+\hat{l}^2}\hat{z}+i(\hat{k}\hat{x}+\hat{l}\hat{y})}d\hat{k}d\hat{l}, \tag{37}$$

where $\hat{x}=(x-c_{g,0}t)/\sigma_x$, $\hat{y}=y/\sigma_y$, $\hat{z}=z/\sigma_x$, and $f(\hat{k},\hat{l})$ is now a bivariate function defined as:

$$f(\hat{k},\hat{l})=\frac{\int_{-\infty}^{\infty}\int_{-\infty}^{\infty}|A(x,y)|^2e^{-i(kx+ly)}dxdy}{\sigma^2|a_0|^2}, \tag{38}$$

where $\hat{k}=k\sigma$ and $\hat{l}=l\sigma$. We have $f(\hat{k},\hat{l})=\pi\exp(-(\hat{k}^2+\hat{l}^2)/4)$ for a bivariate Gaussian group $A(x,y)=a_0\exp(-(\hat{x}^2+\hat{y}^2)/2)$. Obviously, the third dimension generally reduces the magnitude of the return flow (see Figure 3), as the mass imbalance caused by the Stokes transport can be remedied by a return flow in three dimensions rather than one constrained to a plane.

The far-field behavior of the horizontal velocity for such a group (see Appendix B2) is given by a dipole solution in three dimensions:

$$u_{\mathrm{RF}}=\frac{\omega_0|a_0|^2}{4\sigma}\frac{2\hat{x}^2-\hat{y}^2-\hat{z}^2}{(\hat{x}^2+\hat{y}^2+\hat{z}^2)^{5/2}}. \tag{39}$$

At the center of the group ($\hat{x}=0$, $\hat{y}=0$), the horizontal velocity decays with depth as $\hat{z}^{-3}$, evidently a faster rate of decay with depth compared to the two-dimensional case ($\hat{z}^{-2}$). At the surface ($\hat{z}=0$) and at the center of the group ($\hat{x}=0$), the far-field decay with the span-wise coordinate y is equivalent to the decay with depth: $\hat{y}^{-3}$. The horizontal velocity generally decays faster with depth for the three-dimensional case and is also generally smaller in magnitude.

4.1.1. Lagrangian Transport

From (34), we can obtain for the total horizontal Lagrangian transport by the Stokes drift alone, as a function of the initial particle coordinates y_0 and z_0:

$$\Delta x_{\mathrm{SD}}(y_0,z_0)=2\sqrt{\pi}\sigma\alpha^2e^{2k_0z_0}e^{-(y_0/\sigma)^2}, \tag{40}$$

where the only difference with the analogous two-dimensional result (13) is the additional dependence on the transverse (across-group) direction y, given here for a Gaussian group. From (35), we obtain for the net horizontal transport by the return flow as a function of the initial particle coordinates y_0 and z_0:

$$\Delta x_{\mathrm{RF}}=-\frac{\alpha^2}{4\pi^2k_0}\int_{-\infty}^{\infty}\int_{-\infty}^{\infty}\int_{-\infty}^{\infty}\frac{\hat{k}^2 f(\hat{k},\hat{l})}{\sqrt{\hat{k}^2+\hat{l}^2}}e^{\sqrt{\hat{k}^2+\hat{l}^2}\hat{z}_0+i(\hat{k}\hat{x}+\hat{l}\hat{y}_0)}d\hat{k}d\hat{l}d\hat{x}. \tag{41}$$

At the still water level ($z_0=0$) and at the center of the group ($y_0=0$), we obtain from numerical integration of (41): $\Delta x_{\mathrm{RF}}\approx-0.0101\alpha^2/k_0$, approximately a factor of 11.3 smaller than the two-dimensional case (cf. $\Delta x_{\mathrm{RF}}\approx-0.1134\alpha^2/k_0$ for 2-D) thus illustrating the strong weakening effect of three-dimensionality on the return flow.

4.1.2. The Transition Depth and Width

Upon introducing a third dimension, one length scale, i.e., the transition depth, is no longer sufficient to map out the transition between forward transport by Stokes drift and backward transport by the return flow. Assuming that the return flow varies much more slowly spatially than the Stokes drift, an assumption which was shown to be valid for the transition depth of two-dimensional seas, we obtain a parabolic relationship for the transition curve $\Delta x_{\mathrm{L}}\approx\Delta x_{\mathrm{SD}}(y_0^*,z_0^*)+\Delta x_{\mathrm{RF}}(0,0)=0$:

$$k_0z_0^*-\frac{1}{2}\varepsilon^2(k_0y_0^*)^2=\frac{1}{2}\log(\varepsilon)-2.93, \tag{42}$$

which is illustrated in Figure 6a by comparing to the full (y, z) field of Δx_{L} without making this assumption, finding excellent agreement. We define the transition depth and the transition width as intersections with the z axis and the x axis, respectively:

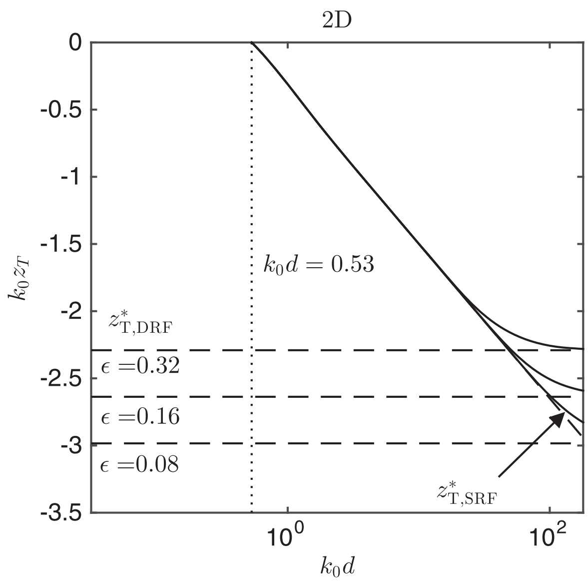

Figure 5. Transition depth for two-dimensional seas comparing the approximate transition depth for deep water ($z^*_{\mathrm{T,DRF}}$) (18) and the approximate transition depth for a shallow return flow ($z^*_{\mathrm{T,SRF}}$) (32) to the implicit solution of $\Delta x_L(z_T)=0$ for three values of $\varepsilon=1/(k_0\sigma)$.

$$z^*_{\mathrm{T,DRF,3D}}=\frac{1}{2k_0}(\log(\varepsilon)-5.86), \tag{43a}$$

$$y^*_{\mathrm{T,DRF,3D}}=\pm\sigma\sqrt{5.86-\log(\varepsilon)}. \tag{43b}$$

Figure 7 compares these approximate length scales to the full solutions demonstrating near-perfect agreement for a broad range of bandwidths.

4.2. Finite Depth ($\sigma_y=\sigma_x$)

Combing the effects of finite depth (section 3) and that of adding the third dimension (section 4.1), gives for the linear signal ($O(\alpha^1\varepsilon^0)$):

$$\eta^{(1)}=A(X,Y)e^{i(k_0x-\omega_0t)}, \tag{44}$$

$$\phi^{(1)}=B(X,Y,Z)\frac{\cosh(k_0(z+d))}{\cosh(k_0d)}e^{i(k_0x-\omega_0t)}, \tag{45}$$

where the slow scales are defined as in (6) and $Y=\varepsilon_y y$ with $\varepsilon_y\equiv 1/(k_0\sigma_y)=\varepsilon_x=\varepsilon$ as in section 4.1. From the linear (in α) free surface boundary conditions (4), we have $B_{z=0}=-igA/\omega_0$ and $\omega_0^2=gk_0\tanh(k_0d)$, the linear dispersion relationship.

From the linear signal (44) and (45), expressions for the Stokes drift and the Stokes transport can be obtained:

$$u_{\mathrm{SD}}=\frac{\omega_0k_0}{2}\frac{\cosh(2k_0(d+z))}{\sinh^2(k_0d)}|A(X,Y)|^2, \tag{46}$$

$$Q_{\mathrm{ST}}=\frac{\omega_0}{2\tanh(k_0d)}|A(X,Y)|^2, \tag{47}$$

where the only difference with their two-dimensional analogs is an additional dependence on y. The leading-order Stokes drift and Stokes transport are only nonzero in the x direction. The return flow is given by:

$$u_{\mathrm{RF}}=-\frac{\omega_0|a_0|^2(1+\delta_{\mathrm{FD}}(k_0d))}{8\pi^2\tanh(k_0d)\sigma}\int_{-\infty}^{\infty}\int_{-\infty}^{\infty}\frac{\hat{k}^2f(\hat{k},\hat{l})}{\sqrt{\hat{k}^2+\hat{l}^2}}\frac{\cosh(\sqrt{\hat{k}^2+\hat{l}^2}(\hat{z}+\hat{d}))}{\sinh(\sqrt{\hat{k}^2+\hat{l}^2}\hat{d})}e^{i(\hat{k}\hat{x}+\hat{l}\hat{y})}d\hat{k}d\hat{l}, \tag{48}$$

where $\hat{k}=k\sigma$, $\hat{l}=l\sigma$, $\hat{x}=(x-c_{g,0})/\sigma$, $\hat{y}=y/\sigma$, $\hat{z}=z/\sigma$, $\hat{d}=d/\sigma$, $\delta_{\mathrm{FD}}(k_0d)$ defined in (24) and $f(\hat{k},\hat{l})$ in (38).

Taking the limit $d/\sigma\to 0$, we obtain a flow that is uniform with depth but varies spatially according to:

$$u_{\mathrm{RF}}=-\frac{\omega_0|a_0|^2(1+\delta_{\mathrm{FD}}(k_0d))}{8\pi^2\tanh(k_0d)d}\int_{-\infty}^{\infty}\int_{-\infty}^{\infty}\frac{\hat{k}^2f(\hat{k},\hat{l})}{\hat{k}^2+\hat{l}^2}e^{i(\hat{k}\hat{x}+\hat{l}\hat{y})}d\hat{k}d\hat{l}. \tag{49}$$

4.2.1. Lagrangian Transport

The net horizontal transport by Stokes drift alone can be found from integrating (46) with respect to time for a Gaussian group. As a function of the initial particle coordinates y_0 and z_0, we obtain:

$$\Delta x_{\mathrm{SD}}=2\sqrt{\pi}\alpha^2\sigma\delta_{\mathrm{SD}}(k_0d)\cosh(2k_0(d+z_0))\exp(-(y_0/\sigma)^2), \tag{50}$$

where $\delta_{\mathrm{SD}}(k_0d)=\coth(k_0d)/(2k_0d+\sinh(2k_0d))$. The only difference with the two-dimensional solution (27) is the additional dependence on $\hat{y}_0=y_0/\sigma$. Similarly, the net displacement by the return flow is given by:

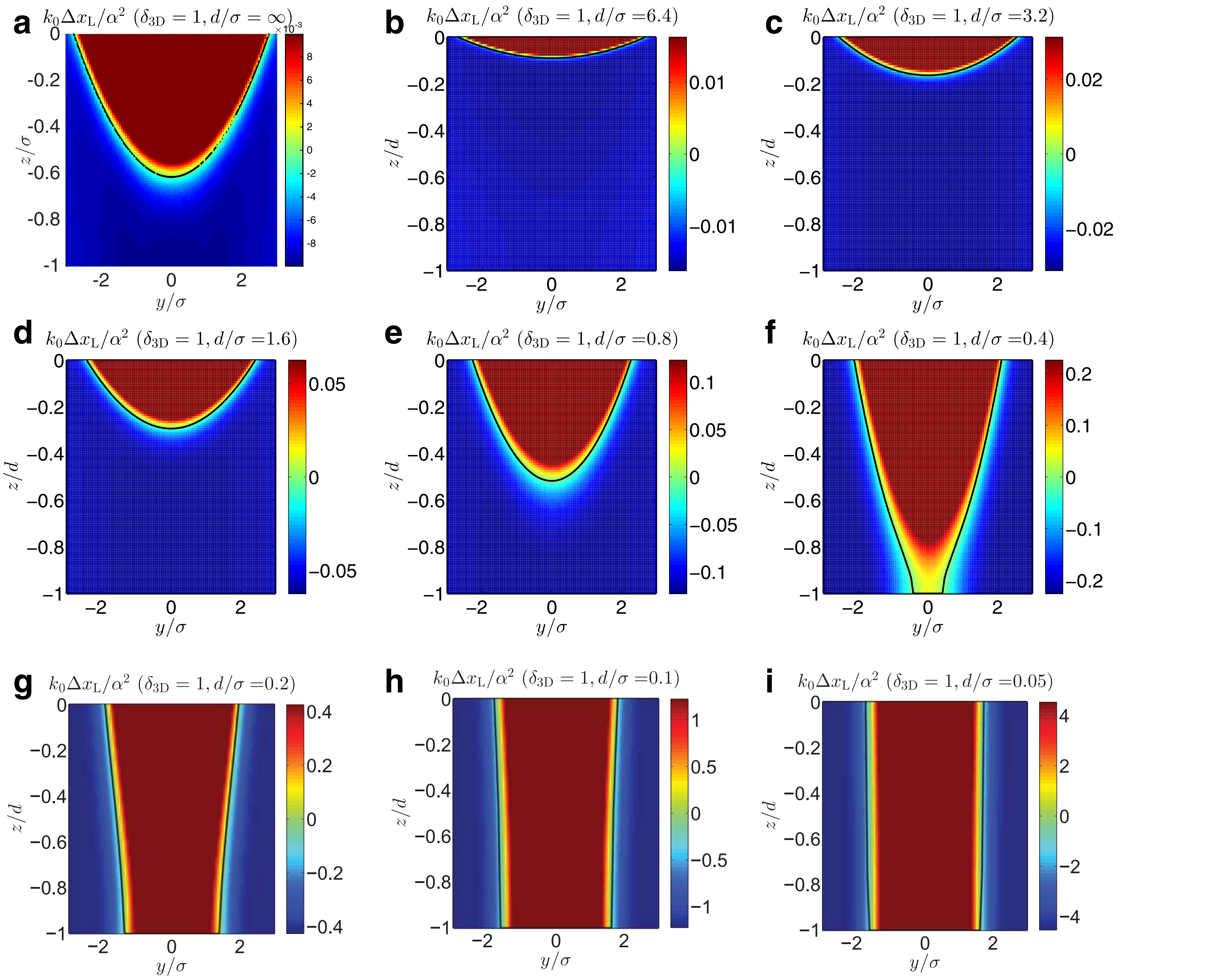

Figure 6. Net horizontal Lagrangian displacement by a three-dimensional wave group with $\sigma\equiv\sigma_x=\sigma_y$ for $\varepsilon=0.16$ and different values for depth $d/\sigma=\{\infty, 6.4, 3.2, 1.6, 0.8, 0.4, 0.2, 0.1, 0.05\}$ ($k_0d=\{\infty, 40, 20, 10, 5, 2.5, 1.25, 0.625, 0.3125\}$ for $\varepsilon=0.16$) showing the approximate transition curve ((42) and (53)) (black line). Note that the color scale saturates for positive $\Delta x_{\rm L}$. Note the vertical axis is scaled differently in Figure 6a.

$$\Delta x_{\rm RF}(y_0,z_0)=-\frac{\alpha^2\delta_{\rm RF}(k_0d)}{4\pi^2k_0}\int_{-\infty}^{\infty}\int_{-\infty}^{\infty}\int_{-\infty}^{\infty}\frac{\hat{k}^2f(\hat{k},\hat{l})}{\sqrt{\hat{k}^2+\hat{l}^2}}\frac{\cosh\left(\sqrt{\hat{k}^2+\hat{l}^2}(\hat{z}_0+\hat{d})\right)}{\sinh\left(\sqrt{\hat{k}^2+\hat{l}^2}\hat{d}\right)}e^{i(\hat{k}\hat{x}+\hat{l}\hat{y}_0)}d\hat{k}d\hat{l}d\hat{x}, \tag{51}$$

with $\delta_{\rm RF}(k_0d)=\delta_{\rm SD}(k_0d)\sinh(2k_0d)(1+\delta_{\rm FD}(k_0d))$ as before. We consider the shallow-water limit $d/\sigma\rightarrow 0$ and obtain from (51):

$$\Delta x_{\rm RF}(y_0)=-\frac{\alpha^2\sigma}{4\pi^2}\frac{\delta_{\rm RF}(k_0d)}{k_0d}\int_{-\infty}^{\infty}\int_{-\infty}^{\infty}\int_{-\infty}^{\infty}\frac{\hat{k}^2f(\hat{k},\hat{l})}{\hat{k}^2+\hat{l}^2}e^{i(\hat{k}\hat{x}+\hat{l}\hat{y}_0)}d\hat{k}d\hat{l}d\hat{x}, \tag{52}$$

where we note that the net transport by the return flow is constant with depth, but remains a function of the transverse coordinate y_0. Figure 4 shows the variation with depth of the net displacement by the return flow for different depths at the center of the group $y=0$, whereas Figure 8 examines its variation with the transverse coordinate y at the still water level $z=0$. It is evident from these figures that the shallow return flow approximation (52) is valid except for extremely large water depths ($k_0d\gtrsim 20$ for $\varepsilon=0.16$).

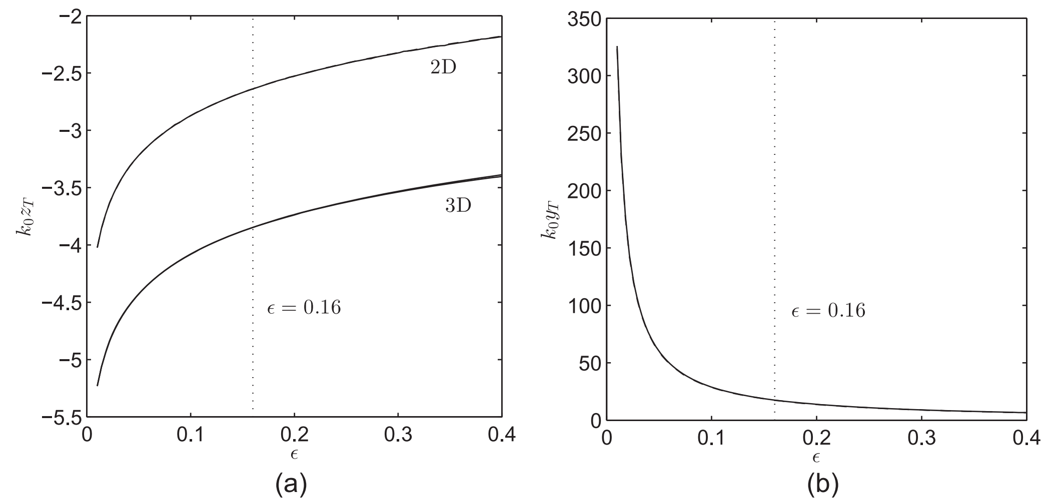

Figure 7. Approximate deep return flow (a) transition depth $z^*_{T,DRF,3D}$ and (b) width $y^*_{T,DRF,3D}$ (43) (dashed lines) compared to the full solutions (continuous lines) for infinite depth and in three-dimensional seas ($\sigma_x = \sigma_x$, $\delta_{3D} = 1$). Note that the full solutions are indistinguishable from the approximate solutions.

4.2.2. The Transition Depth and Width

As before, we can obtain the following approximate relationship for the transition curve: $\Delta x_L \approx \Delta x_{SD}(y_0^*, z_0^*) + \Delta x_{RF}(0,0) = 0$ based on the shallow return flow limit (52). Explicitly, this can be rewritten as:

$$z_0^* = \frac{1}{2k_0}\left(\cosh^{-1}\left(C_{SRF,3D}(\delta_{3D}=1)\frac{\sinh(2k_0 d)(1+\delta_{FD}(k_0 d))}{2k_0 d}e^{(y_0^*/\sigma)^2}\right) - d\right), \tag{53}$$

where the nondimensional constant $C_{SRF,3D}(\delta_{3D}=1)$ is given by:

$$C_{SRF,3D}(\delta_{3D}=1) = \frac{1}{4\pi^{5/2}}\int_{-\infty}^{\infty}\int_{-\infty}^{\infty}\int_{-\infty}^{\infty}\frac{\hat{k}^2 f(\hat{k},\hat{l})}{\hat{k}^2+\hat{l}^2}e^{i(\hat{k}\hat{x}+\hat{l}\hat{y})}d\hat{k}d\hat{l}d\hat{x} \approx 0.056, \tag{54}$$

with the second approximate equality holding for a Gaussian group with $\sigma_x = \sigma_y$.

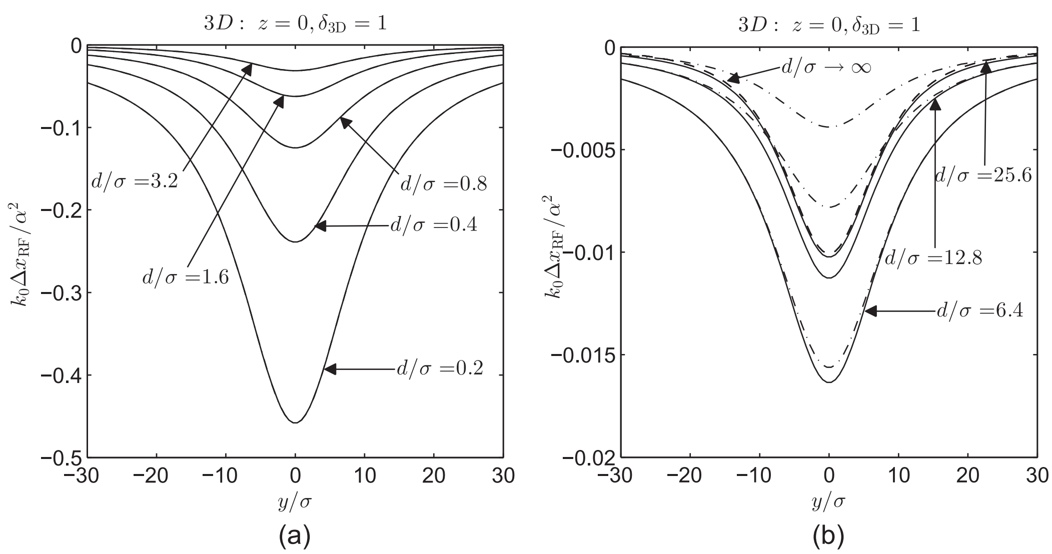

Figure 8. Variation of the net horizontal transport by the return flow in the vertical plane orthogonal to the direction of propagation for different depths. The plot on the left shows intermediate values of depth $d/\sigma = \{3.2, 1.6, 0.8, 0.4, 0.2\}$ ($k_0 d = \{20, 10, 5, 2.5, 1.25\}$ for $\varepsilon = 0.16$) and the plot on the right shows very large depths $d/\sigma = \{\infty, 25.6, 12.8, 6.4\}$ ($k_0 d = \{\infty, 160, 80, 40\}$ for $\varepsilon = 0.16$). Also shown (dash-dotted lines) is the shallow return flow limit (30). The difference is only visible for really large depths (right plots).

Figure 6 illustrates the topology of the transition curve for different depths comparing the finite depth solutions for the net Lagrangian transport Δx_L with the approximate transition curve (53). It is evident from Figure 6 that the transition "curve" is no longer a continuous curve when finite depth effects are considered. In fact, for shallow enough depths and sufficiently spread groups the Stokes drift dominates the return flow at all depths in terms of its net horizontal transport underneath the center of the group. For the case $\delta_{3D}=1$ considered here, this depth criterion corresponds to $k_0d \approx 2.6$ (from $\sinh(2k_0d)(1+\delta_{3D})/(2k_0d)=1/C_{SRF,3D}(\delta_{3D}=1)$). The separation of physical domains that is observed for deep water, in which the Stokes drift dominates near the surface and the return flow at depth is transformed for shallow water provided the group has some directional spreading. In that case, the return flow is dominant everywhere underneath the group ($|y/\sigma|\lesssim 2$) and the return flow dominates everywhere else ($|y/\sigma|\gtrsim 2$). Although we no longer have a parabola, we still define the vertical and horizontal scales of the transition curve as $z^*_{T,SRF,3D} \equiv z^*_0(y^*_0=0)$ and $y^*_{T,SRF,3D} \equiv y^*_0(z^*_0=0)$. We find:

$$z^*_{T,SRF,3D}=\begin{cases} \dfrac{\cosh^{-1}\left(C_{SRF,3D}(\delta_{3D}=1)\dfrac{\sinh(2k_0d)}{2k_0d}\right)}{2k_0}-d & \text{for} \quad \dfrac{\sinh(2k_0d)}{2k_0d}\geq\dfrac{1}{C_{SRF,3D}(\delta_{3D}=1)}, \\ -d & \text{for} \quad \dfrac{\sinh(2k_0d)}{2k_0d}<\dfrac{1}{C_{SRF,3D}(\delta_{3D}=1)}, \end{cases} \tag{55}$$

$$y^*_{T,SRF,3D}=\sigma\sqrt{\log\left(\frac{1}{C_{SRF,3D}(\delta_{3D}=1)}\frac{2k_0d}{\tanh(2k_0d)}\right)}. \tag{56}$$

4.3. Realistic Directional Spectra

Considering more realistic degrees of directional spreading, Appendix C gives the solutions for the three-dimensional return flow field for $\sigma_y \neq \sigma_x$ (and $\delta_{3D}\neq 1$). For different degrees of directional spreading representative of real-world seas, this section then compares the deep and shallow return flow limits of the net displacements of a particle at the free surface and transition depths and width than can be obtained from the velocity fields in Appendix C. We first consider the two limits in turn for $\delta_{3D}\neq 1$.

4.3.1. The Deep Water Return Flow Limit

In deep water ($d/\sigma \rightarrow \infty$), the net transport by Stokes drift and return flow associated with a directionally spread group are given by:

$$\Delta x_{SD}(y_0,z_0)=2\sqrt{\pi}\sigma_x\alpha^2\exp\left(2k_0z_0-\left(\frac{y_0}{\sigma_y}\right)^2\right), \tag{57}$$

$$\Delta x_{RF}(y_0=0,z_0=0)=-\frac{2\sqrt{\pi}C_{DRF,3D}(\delta_{3D})\alpha^2}{k_0}, \tag{58}$$

where $C_{DRF,3D}(\delta_{3D})$ is given by:

$$C_{DRF,3D}(\delta_{3D})=\frac{1}{8\pi^{5/2}}\int_{-\infty}^{\infty}\int_{-\infty}^{\infty}\int_{-\infty}^{\infty}\frac{\hat{k}^2 f(\hat{k},\hat{l})}{\sqrt{\hat{k}^2+\delta_{3D}^2\hat{l}^2}}e^{i(\hat{k}\hat{x}+\hat{l}\hat{y}_0)}d\hat{k}d\hat{l}d\hat{x}. \tag{59}$$

From numerical evaluation of the numerical integral for a Gaussian group, we have for the constant $C_{DRF,3D}=\{0.032, 0.0056, 0.0028, 0.0014, 0.0010\}$ for $\delta_{3D}=\{0, 0.5, 1, 2, 3\}$ with corresponding values of $\Delta x_{RF}(y_0=0, z_0=0)=\{0.1134, 0.0197, 0.0101, 0.0051, 0.0034\}\alpha^2/k_0$ illustrating the dramatic effect of even small degrees of directional spreading on the net horizontal transport by the return flow. The approximate transition curve remains parabolic:

$$k_0z_0-\frac{1}{2}\left(\frac{y_0}{\sigma_y}\right)^2=\frac{1}{2}\log\left(C_{SRF,3D}(\delta_{3D})\varepsilon_x\right). \tag{60}$$

Approximate transition depths and widths are:

$$z^*_{T,DRF,3D}=\frac{1}{2k_0}\left(\log(\varepsilon_x)+\log\left(C_{SRF,3D}(\delta_{3D})\right)\right), \tag{61}$$

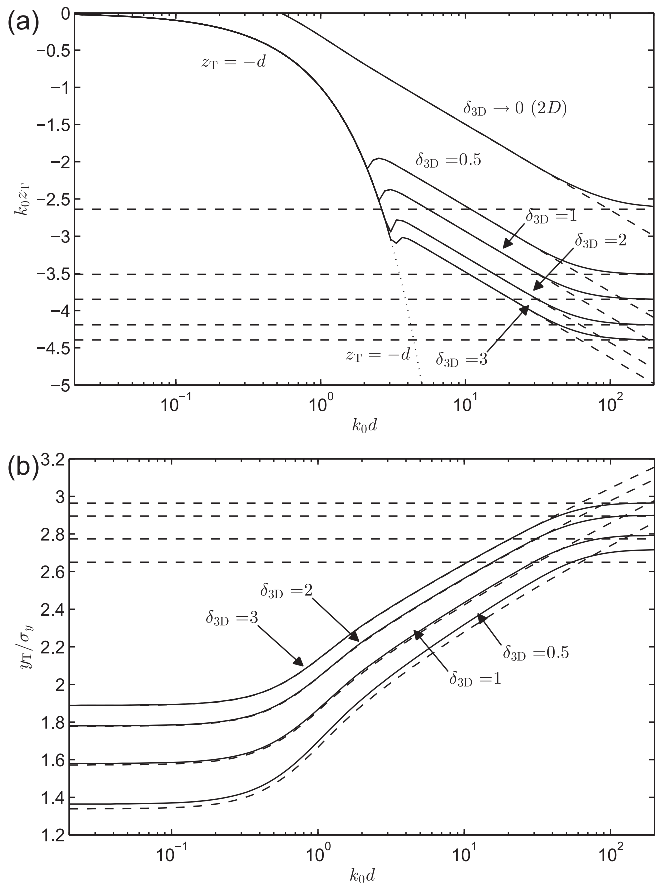

Figure 9. (a) Transition depth and (b) width for three-dimensional seas with different degrees of directionality $\delta_{3D}=\sigma_x/\sigma_y$ and as a function of water depth k_0d. Shown are the deep return flow limit (61) and (62) (horizontal dashed lines), the shallow return flow limit (67) and (68) (dashed lines), and the implicit solution for intermediate depth (continuous lines).

$$y^*_{T,DRF,3D}=\sigma_y\sqrt{-\log\left(C_{SRF,3D}(\delta_{3D})\right)-\log\left(\varepsilon_x\right)}. \tag{62}$$

4.3.2. The Shallow-Water Return Flow Limit

Under the shallow return flow approximation ($d/\sigma \to 0$), the net transport by Stokes drift and return flow associated with a directionally spread group are given by:

$$\Delta x_{SD}(y_0,z_0)=2\sqrt{\pi}\alpha^2\sigma_x\delta_{SD}(k_0d)\cosh\left(2k_0(d+z_0)\right)\exp\left(-(y_0/\sigma_y)^2\right), \tag{63}$$

$$\Delta x_{RF}(y_0=0,z_0=0)=-2\sqrt{\pi}\sigma_x\delta_{SD}(k_0d)(1+\delta_{FD}(k_0d))\frac{\sinh\left(2k_0d\right)}{2k_0d}C_{SRF,3D}(\delta_{3D}), \tag{64}$$

where $C_{SRF,3D}=$ is given by:

$$C_{SRF,3D}(\delta_{3D})=\frac{1}{4\pi^{5/2}}\int_{-\infty}^{\infty}\int_{-\infty}^{\infty}\int_{-\infty}^{\infty}\frac{\hat{k}^2f(\hat{k},\hat{l})}{\hat{k}^2+\delta_{3D}^2\hat{l}^2}e^{i\hat{k}\hat{x}}d\hat{k}d\hat{l}d\hat{x}. \tag{65}$$

From numerical evaluation of the numerical integral for a Gaussian group, we have for the constant $C_{SRF,3D}=\{1, 0.11, 0.056, 0.028, 0.019\}$ for $\delta_{3D}=\{0, 0.5, 1, 2, 3\}$. The approximate transition curve is given by:

$$z_0=\frac{1}{2k_0}\cosh^{-1}\left(\frac{\sinh\left(2k_0d\right)}{2k_0d}C_{SRF,3D}(\delta_{3D})\exp\left((y_0/\sigma_y)^2\right)\right)-d. \tag{66}$$

Approximate transition depths and widths are:

Table 1. Net Horizontal Transport for Particles at the Free Surface and at the Center of the Group ($z_0=0$, $y_0=0$) for Different Depths (Rows) and Different Degrees of Directional Spreading (Columns)[a]

					$\sigma_{RMS}=0^{\circ}$	$\sigma_{RMS}=5^{\circ}$	$\sigma_{RMS}=10^{\circ}$	$\sigma_{RMS}=20^{\circ}$	$\sigma_{RMS}=30^{\circ}$
Location	d	k_0d	$\lvert a_0\rvert$ (m)	Δx_{SD} (m)	Δx_{RF} (m)	Δx_{RF} (m)	Δx_{RF} (m)	Δx_{RF} (m)	Δx_{RF} (m)
Coastal	10 m	0.68	2.9	14.4	−11.9	−1.2	−0.62	−0.31	−0.21
					−11.9	**−1.2**	**−0.62**	**−0.31**	**−0.21**
					−0.07	−0.01	−0.005	−0.003	−0.002
Coastal	20 m	1.0	3.9	14.9	−8.0	−0.82	−0.41	−0.21	−0.14
					−8.0	**−0.82**	**−0.41**	**−0.21**	**−0.14**
					−0.09	−0.01	−0.007	−0.004	−0.002
S. North Sea	40 m	1.7	4.7	18.1	−5.4	−0.56	−0.28	−0.14	−0.09
					−5.4	**−0.56**	**−0.28**	**−0.14**	**−0.09**
					−0.11	−0.02	−0.009	−0.004	−0.003
C. North Sea	80 m	3.2	5.0	21.6	−3.3	−0.34	−0.17	−0.09	−0.06
					−3.3	**−0.34**	**−0.17**	**−0.09**	**−0.06**
					−0.11	−0.02	−0.009	−0.005	−0.003
N. North Sea	160 m	6.4	5.0	22.0	−1.7	−0.17	−0.09	−0.04	−0.03
					−1.7	**−0.18**	**−0.09**	**−0.04**	**−0.03**
					−0.11	−0.02	−0.009	−0.005	−0.003
Continental Slope	500 m	20	5.0	22.0	−0.55	−0.06	−0.03	−0.01	−0.01
					−0.55	**−0.06**	**−0.03**	**−0.01**	**−0.01**
					−0.11	−0.02	−0.009	−0.005	−0.003
Continental Slope	1.0 km	40	5.0	22.0	−0.27	−0.03	−0.01	−0.007	−0.005
					−0.28	**−0.03**	**−0.02**	**−0.008**	**−0.0058**
					−0.11	−0.02	−0.009	−0.005	−0.003
Abyssal Plane	3.0 km	1.2×10^{2}	5.0	22.0	−0.09	−0.009	−0.005	−0.002	−0.001
					−0.14	**−0.02**	**−0.01**	**−0.005**	**−0.003**
					−0.11	−0.02	−0.009	−0.005	−0.003
Abyssal Plane	6.0 km	2.4×10^{2}	5.0	22.0	−0.05	−0.005	−0.002	−0.002	−0.0008
					−0.12	**−0.02**	**−0.009**	**−0.005**	**−0.003**
					−0.11	−0.02	−0.009	−0.005	−0.003
Mariana Trench	11 km	4.4×10^{2}	5.0	22.0	−0.03	−0.003	−0.001	−0.0006	−0.0004
					−0.11	**−0.02**	**−0.009**	**−0.005**	**−0.003**
					−0.11	−0.02	−0.009	−0.005	−0.003

[a]We set $T_0=10$ s, $\alpha=0.2$, and $\varepsilon_x=0.16$. Three values are reported. The top value of Δx_{RF} corresponds to the shallow-water return flow limit, the bold value to the full finite depth solution, and the bottom value to the deep water return flow limit. The root-mean-square spreading parameters $\sigma_{RMS}=\{0^{\circ},5^{\circ},10^{\circ},20^{\circ},30^{\circ}\}$ correspond to $\delta_{3D}=\{0,0.54,1.1,2.2,3.3\}$. If $z_T<-d$, the Stokes drift dominates the return flow at all depths below the center of the group.

$$z^{*}_{T,SRF,3D}=\frac{\cosh^{-1}\left(\frac{\sinh(2k_0d)}{2k_0d}(1+\delta_{FD}(k_0d))C_{SRF,3D}(\delta_{3D})\right)}{2k_0}-d, \tag{67}$$

$$y^{*}_{T,SRF,3D}=\sigma_y\sqrt{-\log\left(C_{SRF,3D}(\delta_{3D})\right)-\log\left(\frac{\tanh(2k_0d)(1+\delta_{FD}(k_0d))}{2k_0d}\right)}, \tag{68}$$

where the transition depth is only defined for $\sinh(2k_0d)(1+\delta_{FD}(k_0d)/(2k_0d)\geq 1/C_{SRF,3D}(\delta_{3D})$. For smaller depths, the Stokes drift is always larger underneath the center of the group.

Figures 9a and 9b compare the transition depth, defined as the solution to $\Delta x_L(y_0=0,z_0=z_T)=0$, and the transition width, defined as the solution to $\Delta x_L(y_0=y_T,z_0=0)=0$, to the approximate scales in the deep return flow limit ($d/\sigma\to\infty$) (61) and (62) and the shallow return flow limit ($d/\sigma\to0$) (67) and (68) for different degrees of directional spreading. It is evident from these figures that the shallow return flow limit provides an excellent approximation except for very large depths. Unless the sea state is perfectly unidirectional, a transition depth cannot be defined for $k_0d\lesssim2$ with all net transport positive below the center of the group. The kinks in Figure 9a arise because of the change in topology of the transition curve as shown in moving from Figures 6e to 6f.

5. Conclusions

This paper has examined the Lagrangian transport by wave groups in finite depth and directionally spread seas driven by two opposing effects: the Stokes transport transporting fluid particles in one direction and

Table 2. Transition Depth at the Center of the Group ($z_0 = 0$, $y_0 = 0$) for Different Depths (Rows) and Different Degrees of Directional Spreading (Columns)[a]

			$\sigma_{RMS}=0^\circ$	$\sigma_{RMS}=5^\circ$	$\sigma_{RMS}=10^\circ$	$\sigma_{RMS}=20^\circ$	$\sigma_{RMS}=30^\circ$
Location	d	k_0d	Z_T (m)	Z_T (m)	Z_T (m)	Z_T (m)	Z_T (m)
Coastal	10 m	0.68	−1.6	$<-d$	$<-d$	$<-d$	$<-d$
			−1.6	**<−d**	**<−d**	**<−d**	**<−d**
			−38.8	−52.2	−57.2	−62.3	−65.2
Coastal	20 m	1.0	−6.4	$<-d$	$<-d$	$<-d$	$<-d$
			−6.4	**<−d**	**<−d**	**<−d**	**<−d**
			−50.9	−68.6	−75.1	−81.7	−85.6
S. North Sea	40 m	1.7	−14.1	$<-d$	$<-d$	$<-d$	$<-d$
			−14.1	**<−d**	**<−d**	**<−d**	**<−d**
			−61.4	−82.8	−90.6	−98.7	−103
C. North Sea	80 m	3.2	−23.1	−51.5	−60.3	−70.9	$<-d$
			−23.1	**−51.5**	**−60.3**	**−70.9**	**<−d**
			−65.3	−88.0	−96.4	−105	−110
N. North Sea	160 m	6.4	−31.8	−60.1	−68.5	−77.1	−82.1
			−31.8	**−60.1**	**−68.5**	**−77.1**	**−82.1**
			−65.5	−88.3	−96.7	−105	−110
Continental slope	500 m	20	−45.9	−74.2	−82.7	−91.3	−96.3
			−45.9	**−74.2**	**−82.7**	**−91.3**	**−96.3**
			−65.5	−88.3	−96.7	−105	−110
Continental slope	1.0 km	40	−54.5	−80.9	−91.3	−99.9	−105
			−54.3	**−80.3**	**−90.7**	**−99.3**	**−104**
			−65.5	−88.3	−96.7	−105	−110
Abyssal Plane	3.0 km	1.2×10^2	−68.2	−96.5	−105	−113	−119
			−63.2	**−87.9**	**−96.3**	**−105**	**−110**
			−65.5	−88.3	−96.7	−105	−110
Abyssal Plane	6.0 km	2.4×10^2	−76.8	−105	−114	−122	−127
			−64.9	**−88.3**	**−96.7**	**−105**	**−110**
			−65.5	−88.3	−96.7	−105	−110
Mariana Trench	11 km	4.4×10^2	**−65.5**	**−88.3**	**−96.7**	**−105**	**−110**
			−65.5	−88.3	−96.7	−105	−110

[a]We set $T_0 = 10$ s and $\varepsilon_x=0.16$. Three values are reported. The top value of Δx_{RF} corresponds to the shallow return flow limit, the bold value to the full finite depth solution and the bottom value to the deep return flow limit. The root-mean-square spreading parameters $\sigma_{RMS}=\{0^\circ, 5^\circ, 10^\circ, 20^\circ, 30^\circ\}$ correspond to $\delta_{3D}=\{0, 0.54, 1.1, 2.2, 3.3\}$.

the return flow opposing this by transporting fluid particles in the opposite direction. Both the effect of finite depth and the effect of directional spreading are crucial factors in determining the magnitude and physical importance of the net transport.

To illustrate these findings, Table 1 shows estimates of the net transport of a particle located at the still water level for a broad range of water depths ranging from shallow coastal regions ($d = 10$ m) to the deepest point in the ocean ($d = 11$ km). The displacements reported in Table 1 are those by one single wave group and can be obtained from integrating the velocity field of both the Stokes drift and the return flow from $t \rightarrow -\infty$ to $t \rightarrow \infty$. Specifically, the values reported for the net displacement by the Stokes drift are given by (50). For the net displacement by the return flow for each water depth and each degree of directional spreading, three values are reported: the top value corresponds to the shallow-water return flow limit (64), the middle (bold) value to the general finite depth solution obtained from integration of the velocity field corresponding to (C3) and the bottom value to the deep water limit (58). The values shown correspond to a wave group of steepness $\alpha=k_0|a_0|=0.2$, a bandwidth parameter of $\varepsilon_x=0.16$ corresponding to the best fit of a Gaussian to a Jonswap spectrum [*Gibbs and Taylor*, 2005] and a peak period of $T_0 = 10$ s. It is evident from this table that the effects of depth on the magnitude of the transport by the return flow are large. Evidently, the limits of validity of a Stokes expansion are reached for sufficiently small depth, when the ratio of depth and wave amplitude $d/|a_0|$ is no longer large. Different authors have studied the range of validity of Stokes theory [*Dean*, 1970; *Hedges*, 1995; *Fenton*, 1990; *Sobey*, 2012]. Typically, the shallow-water limit of validity can be expressed in terms of the Ursell number [*Ursell*, 1953]:

$$U_r=\frac{H\lambda_0^2}{d^3}, \tag{69}$$

where $H = 2a_0$ is the wave height. *Hedges* [1995], for example, shows that $U_r = 40$ gives a good boundary between the validity of Stokes and Cnoidal theory. Using the small parameters in this paper, we have from

(69): $U_r = 8\pi^2\alpha/(k_0 d)^3$. Therefore, $U_r = 40$ and $\alpha = 0.2$ corresponds to $k_0 d \approx 0.73$ and only our estimates for $d = 10$ m in Table 1 are perhaps marginally outside of the domain of validity of Stokes theory. Furthermore, by comparing estimates based on the shallow return flow limit and the deep return flow limit to the general finite depth solution, we show that the return flow can be modeled a uniform flow with depth (the shallow return flow limit) for water depths up to 0.5–1 km for the case considered in Table 1.

Also shown in Table 1 is the effect of directional spreading on the return flow, demonstrating the large decreasing effect of even a small degree of directional spreading on the magnitude of the transport by the return flow. The values of the root-mean-square spreading parameter (15°–30°) shown correspond to the typical range observed in field measurements for storm-driven waves [*Donelan et al.*, 1985; *Ewans*, 1998].

Finally, Table 2 provides an overview of estimates of the transition depth, defined as the depth at which the Lagrangian transport by the Stokes drift and the return flow exactly balance and $\Delta x_L = 0$, for a broad range of water depths. As for Table 1, three values are shown: the shallow return flow limit (67) on top, followed by the general finite depth solution obtained from solution of the implicit equation for $\Delta x_L = 0$ in bold and the deep water limit (61) at the bottom. Again, the effect of directional spreading is significant and for sufficiently shallow water the transition depth cannot be defined, as the return flow is located around instead of below the group.

Although the present paper has only aimed to study the particle displacement by a single wave group, its results, namely the large dependence on depth and directionality, have implications for Stokes drift as forcing of wave-driven upper ocean mixing. In line with our findings, *Webb and Fox-Kemper* [2015] have very recently found a large impact of wave spreading and multidirectional waves on estimates of Stokes drift from data also identifying depth effects. Building on from work in *Breivik et al*. [2014] multichromatic wave are considered. The present study sheds light on the role of the return flow that then complements the Stokes drift and it is clear that at least from the perspective of Lagrangian particles near the surface, its role is small especially when the sea is directionally spread, unless the observer is in a coastal region and the water depth is shallow.

Appendix A: The Shallow-Water Limit

A1. Two-Dimensional Shallow-Water Limit

In the shallow-water limit $k_0 d \to 0$, the linear signal (19) becomes:

$$u^{(1)} = \frac{gk_0}{\omega_0} A(X) e^{i(k_0 x - \omega_0 t)}, \tag{A1a}$$

$$w^{(1)} = -i\frac{gk_0}{\omega_0} k_0 (d+z) A(X) e^{i(k_0 x - \omega_0 t)}, \tag{A1b}$$

with the linear dispersion equation $\omega_0 = \sqrt{gd}k_0$ and $\eta^{(1)} = A(X)\exp\left(i(k_0 x - \omega_0 t)\right)$. The velocity field in (A1) still satisfies conservation of volume. The Stokes drift and transport are given by:

$$u_{SD} = \frac{|A(X)|^2}{2}\sqrt{\frac{g}{d^3}}, \tag{A2a}$$

$$Q_{ST} = \frac{|A(X)|^2}{2}\sqrt{\frac{g}{d}}. \tag{A2b}$$

It is evident that the limit $k_0 d \to 0$ must be taken with great care and that, in such a limit, we must also have $\alpha \to 0$. In physical terms, finite amplitude waves cannot exist on a infinitely thin fluid. From (26), we have:

$$u_{RF} = -\frac{3}{2}\frac{|A(X)|^2}{2}\sqrt{\frac{g}{d^3}}. \tag{A3}$$

The only net contribution to Lagrangian transport then results from the mean set-down ($\partial\eta^{(2)}/\partial t$) and we have $u_L = u_{SD} + u_{RF} = -(|A(X)|^2/4)\sqrt{g/d^3}$, a negative uniform flow. This result is perhaps intuitive, as in the limit of shallow depth the group and phase velocities become equal. In physical terms, individual waves then no longer move through the group taking particles with them and hence cannot drive the irrotational circulation of Stokes drift and return flow associated with deep water wave groups.

A2. Three-Dimensional Shallow-Water Limit

As before, the leading-order Stokes drift and transport are readily extended to three dimensions:

$$u_{SD} = \frac{|A(X,Y)|^2}{2}\sqrt{\frac{g}{d^3}}, \tag{A4a}$$

$$Q_{ST} = \frac{|A(X,Y)|^2}{2}\sqrt{\frac{g}{d}}. \tag{A4b}$$

Taking note of the return flow "forcing equation" (21), conservation of volume can be satisfied in a two-dimensional (x, y) domain to give:

$$u_{RF} = -\frac{1}{2\pi d}\int_{-\infty}^{\infty}\int_{-\infty}^{\infty}\frac{m(x^*,y^*)(x+x^*)}{(x+x^*)^2+(y+y^*)^2}dx^*dy^*, \tag{A5}$$

where $m(x^*, y^*)$ is the source strength of a distribution of sources (and sinks) located at $z = 0$. We have used $\delta_{FD}(k_0 d) \to 1/2$ as $k_0 d \to 0$. Their strength is given by:

$$m(x^*,y^*) = \frac{3}{2}\frac{\partial Q_{ST}(x^*,y^*)}{\partial x^*} = \frac{3}{2}\sqrt{\frac{g}{d}}\frac{|a_0|^2}{\sigma}\frac{x^*}{\sigma}e^{-((x^*/\sigma)^2+(y^*/\sigma)^2)}, \tag{A6}$$

where we have used a summation of dipoles to solve Laplace subject to the boundary condition at $z = 0$ (21) (see Appendix B). The second identity in (A6) holds for a Gaussian group with $\sigma \equiv \sigma_x = \sigma_y$.

Appendix B: The Deep Water Return Flow as a Summation of Sources and Sinks

B1. Two-Dimensional Summation of Sources and Sinks

From the potential of a source with strength M in a two-dimensional infinite half-space located at $x = x^*$ and $z = 0$, $\phi_{RF} = (M/\pi)\ln(\sqrt{(x-x^*)^2+z^2})$, we obtain for the horizontal velocity of a dipole with strength m per unit length and its source and sink located at $x = x^*$ and $x = -x^*$, respectively:

$$du_{RF} = \frac{m}{\pi}\left[\frac{x-x^*}{(x-x^*)^2+z^2} - \frac{x+x^*}{(x+x^*)^2+z^2}\right]dx^*, \tag{B1}$$

from which the return flow field can be found by integrating with respect to x^* from $x^* = 0$ to $x^* \to \infty$. The far-field limit, valid for either $|x| \gg \sigma$, $|z| \gg \sigma$ or both, is:

$$u_{RF} = \frac{2}{\pi}\frac{x^2-z^2}{(x^2+z^2)^2}\int_0^{\infty} m(x^*)x^*dx^* = \frac{1}{2\sqrt{\pi}}\frac{\omega_0|a_0|^2}{\sigma}\frac{\hat{x}^2-\hat{z}^2}{(\hat{x}^2+\hat{z}^2)^2}, \tag{B2}$$

where we have used $\hat{x} = x/\sigma$ and $\hat{z} = z/\sigma$ and the second identity holds for a Gaussian spectrum:

$$m = \frac{\partial Q_{ST}(x^*)}{\partial x^*} = \frac{\omega_0|a_0|^2}{\sigma}\frac{x^*}{\sigma}\exp(-(x^*/\sigma)^2). \tag{B3}$$

B2. Three-Dimensional Summation of Sources and Sinks ($\sigma_x = \sigma_y$)

From the potential of source with strength in a three-dimensional infinite half-space located at (x^*, y^*), $\phi_{RF} = -(M/(2\pi))/\sqrt{(x-x^*)^2+(y-y^*)^2+z^2}$, we obtain for the horizontal velocity of a dipole with its source located at (x^*, y^*) and its sink at $(-x^*, y^*)$:

$$du_{RF} = \frac{m}{2\pi}\left[\frac{x-x^*}{\left((x-x^*)^2+(y-y^*)^2+z^2\right)^{3/2}} - \frac{x+x^*}{\left((x+x^*)^2+(y-y^*)^2+z^2\right)^{3/2}}\right]dx^*dy^*, \tag{B4}$$

from which the return flow field can be found by integrating with respect to x^* from $x^* = 0$ to $x^* \to \infty$ and with respect to y^* from $y^* \to -\infty$ to $y^* \to \infty$. The far-field limit valid for $|x| \gg \sigma$, $|y| \gg \sigma$, and $|z| \gg \sigma$ is:

$$u_{RF} = \frac{2x^2-y^2-z^2}{(x^2+y^2+z^2)^{5/2}} \int_0^\infty \int_0^\infty \frac{2m(x^*,y^*)x^* dx^* dy^*}{\pi} \\ = \frac{\omega_0|a_0|^2}{4\sigma} \frac{2\hat{x}^2-\hat{y}^2-\hat{z}^2}{(\hat{x}^2+\hat{y}^2+\hat{z}^2)^{5/2}}, \tag{B5}$$

where the second identity holds for a Gaussian spectrum:

$$m(x^*,y^*) = \frac{\partial Q_{ST}(x^*,y^*)}{\partial x^*} \frac{\omega_0|a_0|^2}{\sigma} \frac{x^*}{\sigma} \exp\left(-(x^*/\sigma)^2-(y^*/\sigma)^2\right). \tag{B6}$$

Appendix C: Three-Dimensional Return Flow With $\sigma_x \neq \sigma_y$

C1. Infinite Depth ($\sigma_x \neq \sigma_y$)

The assumption $\sigma_x=\sigma_y$ (and $\delta_{3D}=1$) has been relaxed in section 4.3 to examine the effects of realistic degrees of directional spreading. The corresponding solution for the return flow velocity potential with $\delta_{3D} \neq 1$ is:

$$\phi_{RF} = \frac{i\omega_0|a_0|^2}{8\pi^2} \int_{-\infty}^{\infty} \int_{-\infty}^{\infty} \frac{\hat{k} f(\hat{k},\hat{l})}{\sqrt{\hat{k}^2+\hat{l}^2\delta_{3D}^2}} e^{\sqrt{\hat{k}^2+\hat{l}^2\delta_{3D}^2}\hat{z}+i(\hat{k}\hat{x}+\hat{l}\hat{y})} d\hat{k} d\hat{l}, \tag{C1}$$

where $\hat{x}=x/\sigma_x$, $\hat{y}=y/\sigma_y$, $\hat{z}=z/\sigma_x$, and $f(\hat{k},\hat{l})$ is now a bivariate function defined as:

$$f(\hat{k},\hat{l}) = \frac{\int_{-\infty}^{\infty} \int_{-\infty}^{\infty} |A(x,y)|^2 e^{-i(kx+ly)} dx dy}{\sigma_x \sigma_y |a_0|^2}, \tag{C2}$$

where $\hat{k}=k\sigma_x$ and $\hat{l}=l\sigma_y$. We have $f(\hat{k},\hat{l})=\pi \exp\left(-(\hat{k}^2+\hat{l}^2)/4\right)$ for a bivariate Gaussian group $A(x,y)=a_0 \exp\left(-(\hat{x}^2+\hat{y}^2)/2\right)$.

C2. Finite Depth $\sigma_x \neq \sigma_y$

For finite depth, the corresponding solution for the return flow is:

$$\phi_{RF} = \frac{i\omega_0|a_0|^2(1+\delta_{FD}(k_0 d))}{8\pi^2 \tanh(k_0 d)} \int_{-\infty}^{\infty} \int_{-\infty}^{\infty} \frac{\hat{k} f(\hat{k},\hat{l})}{\sqrt{\hat{k}^2+\hat{l}^2\delta_{3D}^2}} \frac{\cosh\left(\sqrt{\hat{k}^2+\hat{l}^2\delta_{3D}^2}(\hat{z}+\hat{d})\right)}{\sinh\left(\sqrt{\hat{k}^2+\hat{l}^2\delta_{3D}^2}\hat{d}\right)} e^{i(\hat{k}\hat{x}+\hat{l}\hat{y})} d\hat{k} d\hat{l}, \tag{C3}$$

with $\hat{d}=d/\sigma_x$. In the shallow return flow limit, we obtain:

$$u_{RF} = -\frac{\omega_0|a_0|^2(1+\delta_{FD}(k_0 d))}{8\pi^2 \tanh(k_0 d) d} \int_{-\infty}^{\infty} \int_{-\infty}^{\infty} \frac{\hat{k}^2 f(\hat{k},\hat{l})}{\hat{k}^2+\hat{l}^2\delta_{3D}^2} e^{i(\hat{k}\hat{x}+\hat{l}\hat{y})} d\hat{k} d\hat{l}. \tag{C4}$$

Acknowledgment

Code used to generate results used in this paper will be made available upon request to the main author at tonvandenbremer@gmail.com.

References

Belcher, S. E., et al. (2012), A global perspective on Langmuir turbulence in the ocean surface boundary layer, *Geophys. Res. Lett.*, *39*, L18605, doi:10.1029/2012GL052932.
Breivik, O., J. Bidlot, and P. A. E. M. Janssen (2014), Approximate Stokes drift profiles in deep water, *J. Phys. Oceanogr.*, *44*, 2433–2445.
Dalzell, J. R. (1999), A note on finite depth second-order wave-wave interactions, *Appl. Ocean Res.*, *21*, 105–111.
Dean, R. G. (1970), Relative validities of water wave theories, *J. Waterw. Harbors Coastal Eng. Div. Am. Soc. Civ. Eng.*, *96*(1), 105–119.
Donelan, M. A., J. Hamilton, and W. H. Hui (1985), Directional spectra of wind-generated waves, *Philos. Trans. R. Soc. London A*, *315*, 509–562.
Ewans, K. C. (1998), Observations of the directional spectrum of fetch-limited waves, *J. Phys. Oceanogr.*, *28*, 495–512.
Fenton, J. D. (1990), Nonlinear wave theories, in *Ocean Engineering Science*, edited by B. L. Méhauté and D. M. Hanes, John Wiley, N. Y.
Gibbs, R. H., and P. H. Taylor (2005), Formation of walls of water in fully nonlinear simulations, *Appl. Ocean Res.*, *27*(4), 142–157.
Hedges, T. S. (1995), Regions of validity of analytical wave theories, *Proc. Inst. Civ. Eng., Water Mar. Energy*, *112*, 111–114.
Kinsman, B. (1984), *Wind Waves: Their Generation and Propagation on the Ocean Surface*, Dover, N. Y.
Longuet-Higgins, M., and R. Stewart (1962), Radiation stress and mass transport in gravity waves, with applications to 'surf beats', *J. Fluid Mech.*, *13*, 481–504.
McIntyre, M. E. (1981), On the wave momentum myth, *J. Fluid Mech.*, *106*, 331–347.
Polton, J. A., D. M. Lewis, and S. E. Belcher (2005), The role of wave-induced Coriolis-Stokes forcing on the wind-driven mixed layer, *J. Phys. Oceanogr.*, *35*, 444–457.
Röhrs, J., K. H. Christensen, L. R. Hole, G. Broström, M. Drivdal, and S. Sundby (2013), Observation-based evaluation of surface wave effects on currents and trajectory forecasts, *Ocean Dyn.*, *62*(10–12), 1519–1533.
Sharma, J., and R. G. Dean (1981), Second-order directional seas and associated wave forces, *Proc. Offshore Technol. Conf.*, *4*, 2505–2514.

Journal of Geophysical Research: Oceans 10.1002/2015JC010712

Sobey, R. J. (2012), Steep progressive waves in deep and shallow water, *Proc. Int. Civ. Eng. Eng. Comput. Mech.*, *165*(3), 181–200.
Stokes, G. G. (1847), On the theory of oscillatory waves, *Trans. Cambridge Philos. Soc.*, *8*, 441–455.
Ursell, F. (1953), The long-wave paradox in the theory of gravity waves, *Proc. Cambridge Philos. Soc.*, *49*(4), 685–694.
Webb, A., and B. Fox-Kemper (2015), Impacts of wave spreading and multidirectional waves on estimating Stokes drift, *Ocean Modell.*, in press.